

University of Nebraska - Lincoln

DigitalCommons@University of Nebraska - Lincoln

Vadim Gladyshev Publications

Biochemistry, Department of

2-29-2008

Structure and Catalytic Mechanism of Eukaryotic Selenocysteine Synthase

Oleg M. Ganichkin

Max-Planck-Institut für Biophysikalische Chemie

Xue-Ming Xu

Molecular Biology of Selenium Section, Laboratory of Cancer Prevention, Center for Cancer Research, NCI, National Institutes of Health, Bethesda, Maryland

Bradley A. Carlson

Molecular Biology of Selenium Section, Laboratory of Cancer Prevention, Center for Cancer Research, NCI, National Institutes of Health, Bethesda, Maryland

Heiko Mix

University of Nebraska-Lincoln

Dolph L. Hatfield

Molecular Biology of Selenium Section, Laboratory of Cancer Prevention, Center for Cancer Research, NCI, National Institutes of Health, Bethesda, Maryland

See next page for additional authors

Follow this and additional works at: <https://digitalcommons.unl.edu/biochemgladyshev>



Part of the [Biochemistry, Biophysics, and Structural Biology Commons](#)

Ganichkin, Oleg M.; Xu, Xue-Ming; Carlson, Bradley A.; Mix, Heiko; Hatfield, Dolph L.; Gladyshev, Vadim N.; and Wahl, Markus C., "Structure and Catalytic Mechanism of Eukaryotic Selenocysteine Synthase" (2008). *Vadim Gladyshev Publications*. 96.

<https://digitalcommons.unl.edu/biochemgladyshev/96>

This Article is brought to you for free and open access by the Biochemistry, Department of at DigitalCommons@University of Nebraska - Lincoln. It has been accepted for inclusion in Vadim Gladyshev Publications by an authorized administrator of DigitalCommons@University of Nebraska - Lincoln.

Authors

Oleg M. Ganichkin, Xue-Ming Xu, Bradley A. Carlson, Heiko Mix, Dolph L. Hatfield, Vadim N. Gladyshev, and Markus C. Wahl

Structure and Catalytic Mechanism of Eukaryotic Selenocysteine Synthase^{*S}

Received for publication, November 14, 2007, and in revised form, December 11, 2007. Published, JBC Papers in Press, December 19, 2007, DOI 10.1074/jbc.M709342200

Oleg M. Ganichkin[‡], Xue-Ming Xu[§], Bradley A. Carlson[§], Heiko Mix[¶], Dolph L. Hatfield[§], Vadim N. Gladyshev[¶], and Markus C. Wahl^{‡1}

From the [‡]Max-Planck-Institut für Biophysikalische Chemie, Zelluläre Biochemie/Makromolekulare Röntgenkristallographie, Am Fassberg 11, D-37077 Göttingen, Germany, the [§]Molecular Biology of Selenium Section, Laboratory of Cancer Prevention, Center for Cancer Research, NCI, National Institutes of Health, Bethesda, Maryland 20892, and the [¶]Department of Biochemistry, University of Nebraska, Lincoln, Nebraska 68588

In eukaryotes and Archaea, selenocysteine synthase (SecS) converts *O*-phospho-L-seryl-tRNA^{[Ser]Sec} into selenocysteyl-tRNA^{[Ser]Sec} using selenophosphate as the selenium donor compound. The molecular mechanisms underlying SecS activity are presently unknown. We have delineated a 450-residue core of mouse SecS, which retained full selenocysteyl-tRNA^{[Ser]Sec} synthesis activity, and determined its crystal structure at 1.65 Å resolution. SecS exhibits three domains that place it in the fold type I family of pyridoxal phosphate (PLP)-dependent enzymes. Two SecS monomers interact intimately and together build up two identical active sites around PLP in a Schiff-base linkage with lysine 284. Two SecS dimers further associate to form a homotetramer. The N terminus, which mediates tetramer formation, and a large insertion that remodels the active site set SecS aside from other members of the family. The active site insertion contributes to PLP binding and positions a glutamate next to the PLP, where it could repel substrates with a free α -carboxyl group, suggesting why SecS does not act on free *O*-phospho-L-serine. Upon soaking crystals in phosphate buffer, a previously disordered loop within the active site insertion contracted to form a phosphate binding site. Residues that are strictly conserved in SecS orthologs but variant in related enzymes coordinate the phosphate and upon mutation corrupt SecS activity. Modeling suggested that the phosphate loop accommodates the γ -phosphate moiety of *O*-phospho-L-seryl-tRNA^{[Ser]Sec} and, after phosphate elimination, binds selenophosphate to initiate attack on the proposed aminoacrylyl-tRNA^{[Ser]Sec} intermediate. Based on these results and on the activity profiles of mechanism-based inhibitors, we offer a detailed reaction mechanism for the enzyme.

Organisms that co-translationally incorporate selenocysteine (Sec)² into proteins in response to UGA codons in mRNA are frequently encountered in all three domains of life, prokaryotes, Archaea, and eukaryotes. The human genome contains 25 known genes encoding selenoproteins (1), several of which have essential functions. Selenoprotein biosynthesis requires two specialized metabolic pathways, the first to synthesize Sec and the second to incorporate Sec into proteins. The benefits of selenoproteins, *e.g.* their unique redox and catalytic properties, apparently outweigh selenium toxicity and the burden of maintaining intricate Sec synthetic and decoding machineries.

Notwithstanding some common themes, both Sec synthesis and decoding (for reviews, see Refs. 2–4) differ in bacteria and eukaryotes, and archaeal selenoprotein biosynthesis largely follows the eukaryotic schemes (5). In all organisms a special tRNA^{[Ser]Sec} bearing an anticodon complementary to the UGA codon is central to both processes (6, 7). All tRNA^{[Ser]Sec} species exhibit a number of non-canonical features whereby they are exclusively utilized for the Sec synthesis and Sec insertion pathways (8).

For Sec insertion at UGA codons, selenocysteyl-tRNA^{[Ser]Sec} is recognized by a special elongation factor, SelB in bacteria (9) and EFSec in eukaryotes (10, 11), that replaces EF-Tu and EF-1 α in escorting the aminoacylated Sec-tRNA^{[Ser]Sec} to the ribosome. Bacterial SelB binds a stem-loop structure located within the coding region of selenoprotein mRNAs and directly downstream of a UGA codon (12). Such stem-loop structures thereby act as Sec insertion sequence elements that recode UGA, which normally signals translational termination. In contrast to bacteria, eukaryotic Sec insertion sequence elements are located in the 3'-untranslated regions of selenoprotein mRNAs (13), alleviating the burden of having to maintain functional secondary structures within the coding region and facilitating insertion of more than one Sec into a single protein chain. Such recognition from a distance requires a special adaptor protein, Sec insertion sequence-binding protein 2 (14). Additional factors appear to be involved in UGA recoding in

* This work was supported in part by Deutsche Forschungsgemeinschaft Grant WA1126-2, a grant from the National Institutes of Health, the Intramural Research Program of the National Institutes of Health, NCI, Center for Cancer Research, and the Max-Planck-Society. The costs of publication of this article were defrayed in part by the payment of page charges. This article must therefore be hereby marked "advertisement" in accordance with 18 U.S.C. Section 1734 solely to indicate this fact.

^S The on-line version of this article (available at <http://www.jbc.org>) contains supplemental Fig. S1.

The atomic coordinates and structure factors (code 3BC8, 3BCA, and 3BCB) have been deposited in the Protein Data Bank, Research Collaboratory for Structural Bioinformatics, Rutgers University, New Brunswick, NJ (<http://www.rcsb.org>).

¹ To whom correspondence should be addressed. Tel.: 49-551-201-1046; Fax: 49-551-201-1197; E-mail: mwahl@gwdg.de.

² The abbreviations used are: Sec, selenocysteine; SecS, selenocysteine synthase; P_{Ser}, *O*-phospho-L-serine; P_{Ser}CysS, *O*-phospho-L-serine-cysteine synthase; *afu*, *A. fulgidus*; F₃-Ala, trifluoroalanine; *mmu*, *M. musculus*; PG, propargylglycine; PLP, pyridoxal phosphate; SeP, selenophosphate; *syn*, *Synechocystis*; Trx, thioredoxin; SLA/LP, soluble liver antigen/liver and pancreas antigen; P-loop, phosphate loop.

Structure and Mechanism of Eukaryotic Selenocysteine Synthase

higher organisms. For example, SECp43 was recently found to associate with a Sec-tRNA^{[Ser]^{Sec}}-EFsec complex *in vitro* and to enhance the interaction between EFsec and Sec insertion sequence-binding protein 2 *in vivo* (15). SECp43 also influences the specific post-transcriptional modification of tRNA^{[Ser]^{Sec}} (16). Furthermore, a role for ribosomal protein L30 in Sec decoding on the ribosome has recently surfaced (17).

Sec synthesis invariably takes place on tRNA^{[Ser]^{Sec}} (6, 7, 18), which is initially aminoacylated with serine by seryl-tRNA^{Ser} synthetase (6, 19). The pathways then diverge in the different domains and recapitulate a trend seen with the decoding systems; *i.e.* eukaryotes rely on a more complex ensemble of factors. In bacteria, a pyridoxal phosphate (PLP)-dependent enzyme, selenocysteine synthase (SeI), uses selenophosphate (SeP) to directly convert Ser-tRNA^{[Ser]^{Sec}} into Sec-tRNA^{[Ser]^{Sec}} (20). However, in eukaryotes Ser-tRNA^{[Ser]^{Sec}} is first phosphorylated by *O*-phospho-L-seryl (P_{Ser})-tRNA^{[Ser]^{Sec}} kinase to produce P_{Ser}-tRNA^{[Ser]^{Sec}} (21). Phosphate apparently is required as a leaving group by eukaryotic Sec synthase (SecS), which subsequently gives rise to Sec-tRNA^{[Ser]^{Sec}}. In bacteria SeP is provided by selenophosphate synthetase, SelD (22). Eukaryotes harbor two homologs of SelD, selenophosphate synthetases 1 and 2 (23), but only selenophosphate synthetase 2 can synthesize SeP for Sec synthesis (24).

The molecular identity of eukaryotic/archaeal SecS has only recently been elucidated. An archaeal open reading frame, annotated as SecS, did not act on Ser-tRNA^{[Ser]^{Sec}} or P_{Ser}-tRNA^{[Ser]^{Sec}} (25). RNA-mediated interference technology provided the first direct evidence for an essential role of soluble liver antigen/liver and pancreas antigen (SLA/LP) in selenoprotein biosynthesis (16). SLA/LP was originally identified as the target of autoantibodies from patients with a severe form of autoimmune chronic active hepatitis (26, 27). Indeed, SLA/LP interacted with SECp43 and tRNA^{[Ser]^{Sec}} as detected by co-immunoprecipitation (16, 26, 28). Structural homology modeling predicted that SLA/LP is a PLP-dependent enzyme of the aspartate aminotransferase family (29). Unequivocal evidence that SLA/LP embodied the elusive eukaryotic/archaeal SecS was finally provided independently by two groups (28, 30) who directly demonstrated the conversion of P_{Ser}-tRNA^{[Ser]^{Sec}} to Sec-tRNA^{[Ser]^{Sec}} by the enzyme.

The identification of eukaryotic/archaeal SecS paved the way for understanding the molecular mechanisms underlying its catalytic activity. Xu *et al.* (28) showed that mouse SecS is able to dephosphorylate P_{Ser}-tRNA^{[Ser]^{Sec}}, indicating that aminoacylyl-tRNA^{[Ser]^{Sec}} is a likely intermediate in the reaction. It was also unequivocally established that SecS employs SeP produced by selenophosphate synthetase 2 as the activated selenium donor (24, 28). Apart from these aspects, the enzyme is presently enigmatic. In particular, it is not known (i) how SecS recognizes its two substrates (P_{Ser}-tRNA^{[Ser]^{Sec}} and SeP) and whether binding occurs concomitantly or sequentially, (ii) how SecS differs from related enzymes that recognize low molecular weight amino acid substrates, (iii) whether and how the enzyme discriminates against free P_{Ser}, and (iv) which residues participate in P_{Ser} to Sec conversion on tRNA^{[Ser]^{Sec}}.

Here we report on a combined structural and biochemical analysis of a mammalian SecS which illuminates the above

questions. We determined high resolution crystal structures of SecS from mouse (*mmu*SecS) in which we find that the active site is constructed around a Lys-284-bound PLP cofactor at the interface of two protomers of a close dimer. A SecS-specific N terminus leads to association of two dimers into a homotetramer, which has possible relevance for P_{Ser}-tRNA^{[Ser]^{Sec}} positioning. The active site is complemented by a SecS-specific loop, which is disordered in the absence of ligands but contracts in the presence of a substrate-mimicking phosphate moiety. A glutamate neighboring the PLP cofactor is ideally positioned to deter substrates bearing a free α -carboxyl group. In line with the structural results, we show that changes of phosphate-coordinating residues, which are solely conserved in SecS orthologs, lead to reduced activity of the enzyme and that SecS does not act on free P_{Ser}. Using in addition the response of SecS toward mechanism-based inhibitors, we propose a detailed catalytic mechanism.

EXPERIMENTAL PROCEDURES

Protein Production and Site-directed Mutagenesis—A DNA fragment encoding the full-length *secS* gene from mouse (GenBankTM accession number NM_172490) was amplified and cloned into pETM-13 vector to allow the expression of a C-terminal His₆-tagged protein. The insert was verified by DNA sequencing. The resulting plasmid was termed pETM-13-*secS*.

Rosetta2(DE3) cells were transformed with the pETM-13-*secS* expression construct. Overproduction of the target protein was carried out at 289 K using auto-inducing medium (31). Cells were harvested when the maximum culture density was reached and resuspended in buffer A (50 mM HEPES-NaOH, pH 7.5, 500 mM NaCl, 20 mM imidazole, 2 mM β -mercaptoethanol). 1 mg of lysozyme and 3 μ l of DNase (1 mg/ml) were added per gram of wet cells, and the mixture was incubated for 30 min on ice with stirring. After completing cell rupture by sonication and removing cell debris by centrifugation, soluble fusion protein was captured on a nickel-nitrilotriacetic acid-Sepharose column (Qiagen), washed with buffer B (50 mM HEPES-NaOH, pH 7.5, 1 M NaCl, 20 mM imidazole, 2 mM β -mercaptoethanol), and eluted with a linear gradient of imidazole (20 to 250 mM) in buffer A. Fractions containing *mmu*SecS were pooled, concentrated, and further purified by gel filtration on a Superdex-200 HiLoad 26/60 column (GE Healthcare) equilibrated with buffer C (10 mM HEPES-NaOH, pH 7.5, 500 mM NaCl, 2 mM dithiothreitol). Purified target protein was concentrated to 14 mg/ml using Vivaspin 15 concentrators (30,000 MWCO; Sartorius Vivascience), separated into aliquots, flash-frozen in liquid nitrogen, and stored at 193 K until use. Using the above protocol we obtained \sim 1.5 mg of *mmu*SecS per liter of bacterial culture at a purity of greater than 95% as estimated by SDS-PAGE analysis (see Fig. 1A).

Mutants of *mmu*SecS^{Arg-313} and *mmu*SecS^{Gln-105} were generated in pETM-13-*secS* via the QuikChange protocol (Stratagene). The mutations were verified by DNA sequencing. All mutants of *mmu*SecS were purified in the same way as the wild type protein.

Limited Proteolysis and Analytical Gel Filtration Analysis—50 μ l of *mmu*SecS (14 mg/ml) were incubated with 3 μ g of elastase at 277 K for 80 min. The major band on an SDS gel

originating from elastase treatment (*mmuSecS*^{elast}; see Fig. 1A) was in-gel-digested with trypsin, and fragments were analyzed by matrix-assisted laser desorption ionization-mass spectrometry as described (32).

Analytical gel filtration was conducted on a Superdex-200 PC 3.2/30 size exclusion column (2.4-ml gel bed, column dimensions 3.2 × 300 mm) on a SMART fast protein liquid chromatography system (GE Healthcare). *Escherichia coli* Sela (a decamer of ~506 kDa), *Saccharomyces cerevisiae* cystathionine γ -lyase (a tetramer of ~170 kDa), and *Methanocaldococcus jannaschii* Sela-like protein (MJ0158; a dimer of ~84 kDa) served as size standards.

In Vitro Transcription and Filter Binding Assay—The template for *in vitro* transcription was prepared as described (21). Uniformly ³²P-labeled tRNA^{[Ser]Sec} was transcribed in 50 μ l of transcription buffer (30 mM HEPES-NaOH, pH 8.0, 6.4 mM MgCl₂, 2 mM spermidine, 40 mM dithiothreitol, 400 μ M each of GTP, CTP, and ATP, 200 μ M UTP, 40 μ Ci of [α -³²P]UTP (3000 Ci/mmol), 32 units of RNasin) containing 5 μ g of linearized DNA template and 1.5 μ l of T7 RNA polymerase. The transcription mixture was incubated for 2 h at 310 K, and synthetic tRNA^{[Ser]Sec} was gel-purified.

10,000 cpm (100 fmol) of ³²P-labeled unacylated tRNA^{[Ser]Sec} were incubated 30 min on ice with 2.5, 5, 10, or 20 μ M *mmuSecS* or *mmuSecS*^{elast} in 20 μ l of buffer D (HEPES-NaOH, pH 7.5, 200 mM NaCl, 5 mM MgCl₂, 1 mM dithiothreitol, 0.5 mg/ml total *E. coli* tRNA). 10- μ l aliquots of the reaction mixtures were loaded on a Protran BA 83 nitrocellulose membrane (Whatman) and washed with 50 ml of buffer C. For the detection of RNA-protein complexes, the membrane was exposed to a PhosphorImager screen overnight, which was then scanned using a Typhoon 8600 (GE Healthcare).

SecS Activity Assay—Synthetic tRNA^{[Ser]Sec} was used in all reactions for assaying SecS activity. Synthetic tRNA^{[Ser]Sec} was aminoacylated with serine by seryl-tRNA^{Ser} synthetase, the seryl moiety was phosphorylated (21), and the P-Ser-tRNA^{[Ser]Sec} was isolated (28). The extent of serylation of tRNA^{[Ser]Sec} in the presence of seryl-tRNA^{Ser} synthetase, serine, and other reaction components was 80–90%, and subsequent phosphorylation in the presence of P-Ser-tRNA^{[Ser]Sec} kinase, ATP, and other reaction components neared 100% (Refs. 21 and 28 and references therein).³ The preparations of seryl-tRNA^{Ser} synthetase and P-Ser-tRNA^{[Ser]Sec} were exactly as described elsewhere (see Ref. 21 and references therein). Because less than 20% spontaneous deacylation of the aminoacyl-tRNA^{[Ser]Sec} constituents occurs during their preparation and use (Ref. 21 and references therein), the relative amounts of tRNA^{[Ser]Sec}, seryl-tRNA^{[Ser]Sec}, and P-Ser-tRNA^{[Ser]Sec} used in reactions with SecS generating Sec-tRNA^{[Ser]Sec} can be estimated to be ~45:0:55, respectively, wherein an ~20% deacylation occurs at both steps involving P-Ser-tRNA^{[Ser]Sec} preparation.

The activities of *mmuSecS*^{elast} and of the *mmuSecS* point mutants relative to that of the full-length wild type *mmuSecS* were determined. Thioredoxin (Trx) was used as a negative control. Sec synthetic reactions were carried out as described

(28). The selenium donor, SeP, was generated from chemically synthesized [(CH₃)₃SiO]₃PSe (28), which was a generous gift of Dr. Richard Glass, and 0.2 mM SeP was used in all Sec synthesis assays.

Dephosphorylation Activity of mmuSecS—Dephosphorylation of P-Ser-tRNA^{[Ser]Sec} was carried out as described (28) with the following modifications. In the inhibition assays, *mmuSecS* was incubated with different concentrations of propargylglycine (PG) or trifluoroalanine (F₃-Ala) for 3 min at room temperature in a 10- μ l volume of buffer (28), 100 ng of ³²P-labeled and 1.0 μ g of cold P-Ser-tRNA^{[Ser]Sec} were added to bring the total volume to 20 μ l, and the reaction was incubated at 310 K for 15 min. To assess the activity of *mmuSecS* on free P-Ser, a stock solution of [³²P]P-Ser was prepared by deacylating 0.5 μ g of [³²P]P-Ser-tRNA^{[Ser]Sec} in 25 μ l at pH 9.0 and 315 K for 1 h. 5 μ l of [³²P]P-Ser were added to each of the *mmuSecS* reactions and then incubated for 15 min at 310 K. 10 units of alkaline phosphatase were used to dephosphorylate [³²P]P-Ser, and the resulting phosphate was used as a positive control. Reactions were prepared for chromatography and chromatographed as given (28).

Crystallographic Procedures—For crystallization, 1.5 μ l of *mmuSecS*^{elast} (14 mg/ml in buffer C) were mixed with an equal volume of reservoir solution (11% [v/v] ethylene glycol without other buffer components) in a 24-well Cryschem plate (Hampton Research) immediately after elastase treatment. Crystals were grown by sitting-drop vapor diffusion at 293 K. They appeared overnight and continued to grow for the next 2 days. For data collection, crystals of *mmuSecS*^{elast} were shock-frozen in a 100 K nitrogen stream (Oxford Cryosystems) after transfer into a cryo-protecting buffer (100 mM HEPES-NaOH, pH 7.5, 250 mM NaCl, 1 mM dithiothreitol, 35% (v/v) ethylene glycol). All data were recorded on a Bruker-Nonius FR591 rotating anode generator producing CuK α X-radiation ($\lambda = 1.54179$ Å) at 45 kV and 100 mA equipped with Osmic mirrors and a MAR345 image plate (MARRResearch). Data were processed with the HKL package (33) (Table 1).

The structure of *mmuSecS*^{elast} was solved via a single isomorphous replacement with anomalous scattering strategy. Crystals were soaked for 30 s in cryo-protecting buffer supplemented with 0.5 M sodium iodide and immediately shock-frozen in a 100 K nitrogen stream. Friedel pairs were kept separate during data reduction (Table 1). The iodide-soaked crystals proved isomorphous to the native crystals. 42 iodide positions were found by using SHELXD (34) and used for initial phase calculations (Table 1). Solvent flattening with SHELXE clearly indicated the correct hand of the heavy atom substructure (Table 1) and yielded a high quality experimental electron density map (supplemental Fig. S1).

424 of the 438 residues located in the final structure were positioned in the first round of automatic model building with ARP/wARP (35). The structure was completed by manual model building and automatic refinement with Refmac5 (36). Water molecules were automatically placed with ARP/wARP. One solute species was identified as a chloride ion based on the presence of 250 mM NaCl in the crystallization buffer and residual positive electron density after placement of a water molecule. Another solvent molecule was interpreted as an ethylene

³ X.-M. Xu, B. A. Carlson and D. L. Hatfield, unpublished data.

Structure and Mechanism of Eukaryotic Selenocysteine Synthase

glycol molecule originating from the crystallization or cryo-protecting buffer. TLS refinement (37) was conducted to model differential global anisotropic displacements of the three domains of *mmuSecS^{elast}*. During all stages of refinement, a randomly selected set of 5% of the reflections was used for cross-validation (Table 1). The iodide-soaked crystal structure was refined by the same strategy including the 42 iodide ions located by SHELXD. Additional, lower occupancy iodide positions were found in an anomalous difference Fourier map, obtained with phases calculated from the final refined native structure and the anomalous differences measured for the iodide data set.

For monitoring of phosphate binding, crystals were soaked for 1 min in cryo-protecting buffer supplemented with 0.5 M sodium phosphate, pH 7.5. Similarly, crystals could be derivatized with sulfate (not shown). Data were collected as described, and the structure of a phosphate-soaked crystal was solved by molecular replacement with MOLREP (38) using the structure coordinates of the native protein as a search model while omitting the solvent structure, the PLP cofactor, and alternative side chain conformations. Model building and refinement were conducted as described for the native protein (Table 1). Coordinates and structure factors have been submitted to the Protein Data Bank.

RESULTS

Limited Proteolysis Delineates a SecS Core Fully Active in P_{Ser}-tRNA^{[Ser]_{Sec} to Sec-tRNA^{[Ser]_{Sec} Conversion}}—We expressed, purified, and crystallized full-length SecS from mouse (*mmuSecS*), but the crystals diffracted only to ~6 Å resolution. To explore the possibility that flexible regions hindered generation of well ordered crystals, *mmuSecS* (~55 kDa) was digested with various proteases. Elastase gave rise to a stable fragment of about 49 kDa (Fig. 1A). Tryptic mass spectrometric fingerprinting showed that the elastase-resistant fragment encompassed residues 19–468 (not shown). Thus, the protease removed most of the C-terminal portion that carries the main SLA/LP antigenic epitope (26, 27), also lacking in archaeal SecS (Fig. 2). We refer to the elastase-resistant core of the enzyme as *mmuSecS^{elast}*.

Gel filtration analysis revealed that *mmuSecS* is tetrameric in solution (Fig. 1B). Elastase treatment did not change the migration behavior of the protein detectably, showing that the proteolytic treatment left the quaternary structure of the enzyme intact (Fig. 1B). Because *mmuSecS* binds significantly to unacylated tRNA^{[Ser]_{Sec} (28), we examined the tRNA^{[Ser]_{Sec} binding activity of *mmuSecS^{elast}* by nitrocellulose filter binding. The elastase-treated protein bound tRNA^{[Ser]_{Sec} with an affinity and specificity comparable with those of the full-length enzyme (Fig. 1C). We next tested the Sec synthesis activity of *mmuSecS^{elast}* using a paper chromatographic assay (28). After removal of elastase by gel filtration chromatography, *mmuSecS^{elast}* was incubated with buffer containing SeP and P_{Ser}-tRNA^{[Ser]_{Sec} (obtained by phosphorylation of Ser-tRNA^{[Ser]_{Sec} by P_{Ser}-tRNA^{[Ser]_{Sec}) (21, 28). As positive and negative controls, *mmuSecS* and Trx, respectively, were substituted for *mmuSecS^{elast}*. The efficiency at which *mmuSecS^{elast}* converted P_{Ser}-tRNA^{[Ser]_{Sec} to Sec-tRNA^{[Ser]_{Sec} was indistinguishable from}}}}}}}}

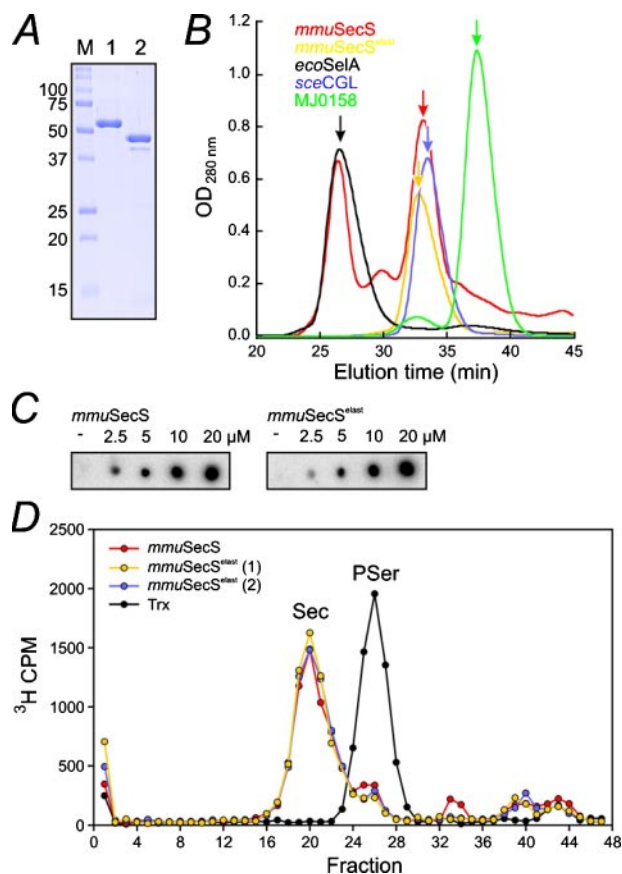


FIGURE 1. Characterization of *mmuSecS^{elast}*. A, SDS-PAGE of *mmuSecS* (lane 1) and *mmuSecS^{elast}* (lane 2). M, molecular weight markers. B, analytical gel filtration analysis of *mmuSecS* (red) and *mmuSecS^{elast}* (gold), *E. coli* SelA (*ecoSelA*) (black, ~506 kDa), *S. cerevisiae* cystathionine γ -lyase (*sceCGL*; blue, ~170 kDa), and MJ0158 (green, ~84 kDa) served as molecular mass markers. Peaks containing the respective proteins (arrows) were verified by monitoring the absorbance at 420 nm and by SDS-PAGE analysis (not shown). The high molecular weight peak (left) represents a contaminating nucleic acid fraction. C, filter binding assay showing similar affinity of *mmuSecS* (top panel) and *mmuSecS^{elast}* (bottom panel) for deacylated tRNA^{[Ser]_{Sec}. Experiments were conducted in the presence of unlabeled competitor tRNA and, thus, represent specific affinities. Concentrations of protein in the reactions are indicated. D, conversion of [³H]P_{Ser}-tRNA^{[Ser]_{Sec} to [³H]Sec-tRNA^{[Ser]_{Sec} by *mmuSecS* (red) and *mmuSecS^{elast}* (gold and blue, which are duplicates, *mmuSecS^{elast}* 1 and *mmuSecS^{elast}* 2). Trx (black) served as a negative control. Details are given under "Experimental Procedures."}}}

that of the full-length enzyme (Fig. 1D). The above results demonstrate that *mmuSecS^{elast}* structurally and functionally closely resembles the full-length enzyme and constitutes a suitable platform on which to explore the structure-activity relationships of SecS-dependent Sec biosynthesis.

SecS Is a Member of the Fold Type I Family of PLP-dependent Enzymes with Distinct Structural Elements—*mmuSecS^{elast}* crystallized readily after the addition of 11% (v/v) ethylene glycol at room temperature. The crystals diffracted to high resolution on a rotating anode x-ray generator and could be derivatized by quick-soaking in 0.5 M sodium iodide for structure solution by single isomorphous replacement with anomalous scattering (Table 1; Fig. S1). Refinement converged at R/R_{free} factors of 16.8/19.8% with the final model exhibiting good overall stereochemistry (Table 1). The only amino acids lacking well defined electron density were residues 19–22 at the N terminus, residue 468 at the C terminus, and residues 98–104, constituting a flexible loop.

Structural homology searches (39) suggested that *mmu*SecS^{elast} exhibits significant similarity to the fold type I family of PLP-dependent enzymes (also referred to as the aspartate aminotransferase family) (40). Where appropriate, we will compare the structure of *mmu*SecS^{elast} to those of *Archaeoglobus fulgidus* P_{Ser}-cysteine synthase (*afu*P_{Ser}CysS) (41), members of the NifS family of Cys/Sec lyases (42–46), and the cystine C-S lyase C-DES from *Synechocystis* (*syn*C-DES) (47). A quantitative comparison with these proteins is given in Table 2. These enzymes act or can act on related substrates and may share some catalytic properties with SecS. In particular, P_{Ser}CysS from methanogenic Archaea affords a precedence for the tRNA-based amino acid synthesis via a P_{Ser}-tRNA intermediate. In these organisms the sole pathway for cysteine biosynthesis is via P_{Ser}-tRNA^{Cys}, obtained by direct aminoacylation of tRNA^{Cys} with P_{Ser} by P_{Ser}-tRNA^{Cys} synthetase, and subsequent P_{Ser}-tRNA^{Cys} to Cys-tRNA^{Cys} conversion by P_{Ser}CysS (48).

*mmu*SecS^{elast} can be divided into three domains (Fig. 3, A and B). Domain 1 (*blue* scaffold in Fig. 3, A and B) is a composite of residues 23–130 and 313–330 and is purely α -helical (encompassing helices α 1– α 4 and α 12). The N terminus (residues 23–44; element I in Fig. 3, A and B) differs from that of other fold type I enzymes (Fig. 3, C and D). In *mmu*SecS^{elast}, helix α 1 is positioned at the protein surface, running approximately perpendicular to the scaffolding helices of the domain. Domain 1 also exhibits a long insertion between helices α 2 and α 4 (residues 62–108; element II in Fig. 3, A and B), which encompasses two loops separated by helix α 3. The corresponding element in other enzymes of the fold type I family is significantly shorter (Fig. 3, C and D). Seven residues within the second loop of the insertion (residues 98–104) are disordered due to intrinsic flexibility (bordered by *spheres* in Fig. 3A). Both the non-canonical N terminus and the unique insertion are conserved among SecS orthologs (Fig. 2) and, therefore, are expected to confer unique functions on the enzyme.

Domain 2 of SecS is the largest module of the protein (residues 131–312; *cyan* scaffold in Fig. 3, A and B). It comprises a $\alpha/\beta/\alpha$ sandwich fold encompassing a seven-stranded β -sheet (β 1– β 9– β 8– β 7– β 6– β 2– β 3) characteristic of the fold type I family. The β -sheet is parallel except for strand β 9 (Fig. 3, A and B). A short helix (α 10) between strands β 8 and β 9 carries a PLP cofactor in Schiff-base linkage to Lys-284 (Figs. 3A and 4). Helices α 7, α 8, and α 9 line the β -sheet at the convex outside, and helices α 5, α 6, and α 11 lie at the concave inside. A short β -hairpin (β 4 and β 5) is inserted between strand β 3 and helix α 7. Domain 2 is connected to the second part of domain 1 by a short loop (residues 311–314; element III in Fig. 3, A and B).

Domain 3 of SecS (residues 331–467; *steel blue* scaffold in Fig. 3, A and B) exhibits an α/β sandwich fold with three almost parallel helices (α 13, α 14, and α 15) on the outside covering an antiparallel three-stranded β -sheet (β 10– β 14– β 11), which in turn rests on top of domain 2. A long loop (residues 408–430; element IV in Fig. 3, A and B) with a β -hairpin (β 12– β 13) at the tip is inserted between strands β 11 and β 14. The three-stranded β -sheet and the β -hairpin of the loop are at approximately right angles and encircle part of domain 2 (Fig. 3A).

Strands β 11 and β 12 thereby form one rim of an active site funnel leading from the surface to the PLP (Fig. 3A). In the NifS-like enzymes, the analog of the long domain 3 loop (element IV) is often disordered (43) and bears a conserved Cys that can be charged in the active site with elemental sulfur. The resulting persulfide is thought to donate a S⁰ building block for iron-sulfur cluster biosynthesis. Element IV of *mmu*SecS^{elast} does not contain a Cys.

Cross-strutting via the N Terminus Leads to Homotetramers That Exhibit Surface Properties Suitable for Binding P_{Ser}-tRNA^{[Ser]Sec}—*mmu*SecS^{elast} crystals contained one protein molecule per asymmetric unit. Consistent with the gel filtration analysis, the orthorhombic crystal symmetry gave rise to tetramers in which the protomers are related by three orthogonal 2-fold axes (see Fig. 5A, left). Within a tetramer, two pairs of monomers (Mol I/II and Mol III/IV; Fig. 5A, left) interact intimately, burying 7343 Å² of combined surface area upon association. Two of these close dimers further associate into tetramers via less extensive interactions between Mol I and Mol III, *viz.* Mol II/Mol IV (1891 Å² combined surface area buried in each contact), and between Mol I and Mol IV, *viz.* Mol II/III (276 Å² combined surface area buried in each contact; Fig. 5A, left). The tetramers are held together by the formation of a short antiparallel coiled-coil between the α 2 helices of Mol I and III (Mol II and IV), which is cross-strutted by helices α 1 (Fig. 5B). In contrast, *afu*P_{Ser}CysS, NifS relatives, or *syn*C-DES lack the surface-exposed N terminus (elements I in Fig. 3, C and D). Consistently, all these latter proteins exist as dimers.

Fig. 5C shows the electrostatic potential mapped to the surface of a *mmu*SecS^{elast} tetramer. Large patches of positive charge (*blue*) are visible, consistent with the overall basic pI of 8.3 calculated for the protein. In particular, the funnel leading to the active site is strongly positively charged. Therefore, the surface properties of *mmu*SecS^{elast} appear to be designed to contact the sugar-phosphate backbone of tRNA^{[Ser]Sec} at multiple positions. Consistent with this view, we observed avid binding of anions to *mmu*SecS^{elast}. After soaking with NaI, we located 62 iodide ions per protomer bound to the surface of *mmu*SecS^{elast} (Fig. 5D). One of these positions was always occupied by a chloride ion in structures not treated with iodide (not shown).

The PLP Cofactor Is Tightly Anchored by Non-canonical Contacts to Both Protomers of a Close Dimer—A close dimer exhibits two identical active sites at the protomer interfaces pinpointed by a PLP cofactor (Fig. 4A). Because the PLP was refined at full occupancy, leaving no residual difference density, all four subunits of a tetramer bear a cofactor. This situation is different from *afu*P_{Ser}CysS, where only one of two potential active sites in a dimer was equipped with PLP (41). We refer to the PLP attached to Lys-284 of a reference molecule and the surrounding active site as “cis”; the PLP attached to the opposite protomer and its surrounding active site are referred to as “trans.”

In *mmu*SecS^{elast}, both monomers of a close dimer contribute side chains for PLP binding in an active site (Fig. 4A). Apart from the covalent linkage to Lys-284, PLP is additionally bound via multiple hydrogen bonds and electrostatic and van der Waals interactions in cis. These interactions

Structure and Mechanism of Eukaryotic Selenocysteine Synthase

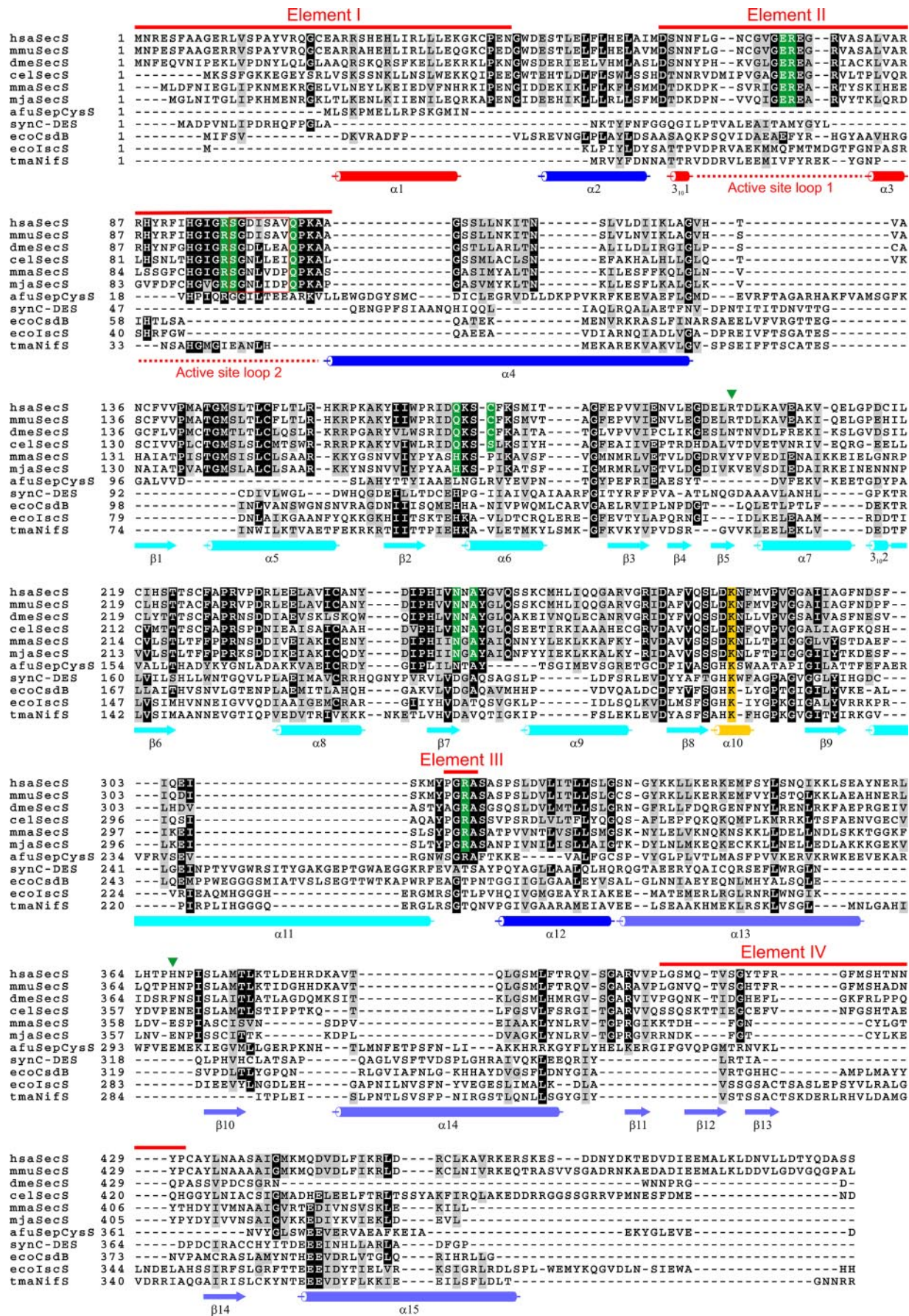


TABLE 1

Crystallographic data

r.m.s.d., root mean square deviation; ESU, estimated overall coordinate error based on maximum likelihood.

	Native	Iodide	Phosphate
Data collection			
Space group	I222	I222	I222
Unit cell parameters (<i>a</i> , <i>b</i> , <i>c</i> ; Å)	59.2, 138.7, 141.7	59.2, 138.4, 141.5	59.2, 138.7, 141.7
Resolution (Å)	30.0-1.65 (1.74-1.65) ^a	50.0-2.25 (2.38-2.25) ^a	50.0-1.85 (1.95-1.85)
Reflections			
Unique	68,502 (9,938)	52,394 (7,738)	49,649 (7,322)
Completeness (%)	97.3 (95.3)	98.3 (97.0)	99.3 (99.2)
Redundancy	4.7 (4.5)	4.7 (4.7)	3.5 (3.1)
<i>I</i> / σ (<i>I</i>)	20.5 (2.1)	13.4 (3.8)	16.3 (1.90)
$R_{\text{sym}}(I)^b$	0.045 (53.9)	0.093 (35.4)	0.046 (54.2)
Phasing			
Resolution (Å)	30.0-2.0		
Heavy atom sites	42		
Correlation coefficients ^c			
SHELXD CC _{all} /CC _{weak}	50.86/37.73		
SHELXE CC _{overall}	35.52		
CC _{free} left/right hand	62.69/26.92		
FOM ^d	0.582		
Refinement			
Resolution (Å)	20.0-1.65 (1.69-1.65)	30.0-2.25 (2.31-2.25)	20.0-1.85 (1.99-1.85)
Reflections			
Number	65,002 (4,662)	26,104 (1,839)	47,049 (3,157)
Completeness (%)	97.3 (95.0)	98.0 (96.3)	98.8 (93.0)
Test set (%)	5.1	5.0	5.1
R_{work}^e	0.168 (0.390)	0.183 (0.199)	0.166 (0.341)
R_{free}^e	0.198 (0.401)	0.237 (0.303)	0.202 (0.372)
ESU (Å)	0.061	0.129	0.077
Contents of asymmetric unit			
Protein molecules/residues/atoms	1/433/3647	—/—/—	1/441/—
Water oxygens	723	264	509
PO ₄ ³⁻ /Cl ⁻ /I ⁻	—/1/—	—/—/50	2/1/—
Mean B-factors (Å ²)			
Wilson	20.0	32.2	23.9
Protein	15.1	26.9	21.0
Water	38.4	28.7	38.2
Ions	16.5	45.9	45.9
Ramachandran Plot ^f			
Favored	97.9 (424/433)	97.7 (421/431)	97.7 (431/441)
Allowed	1.9 (8/433)	2.1 (9/433)	2.3 (10/441)
Outliers	0.2 (1/433)	0.2 (1/433)	0.0
r.m.s.d. target geometry			
Bond lengths (Å)	0.012	0.010	0.010
Bond angles (°)	1.34	1.22	1.19
r.m.s.d. B-factors (Å ²)			
Main chain bonds	0.726	0.423	0.563
Main chain angles	1.122	0.787	0.894
Side chain bonds	2.005	1.402	1.604
Side chain angles	3.152	2.318	2.540

^a Data for the highest resolution shell in parentheses.^b $R_{\text{sym}}(I) = \sum_{\text{hkl}} \sum_i |I_i(\text{hkl}) - \langle I(\text{hkl}) \rangle| / \sum_{\text{hkl}} \sum_i I_i(\text{hkl})$ for *n* independent reflections and *i* observations of a given reflection; $\langle I(\text{hkl}) \rangle$, average intensity of the *i* observations.^c $CC = [\sum_w E_o E_c \sum_w - \sum_w E_o \sum_c E_c] / \{[\sum_w E_o^2 \sum_w - (\sum_w E_o)^2][\sum_w E_c^2 \sum_w - (\sum_w E_c)^2]\}^{1/2}$; *w*, weight (see SHELX software for full definitions).^d Figure of merit (FOM) = $|F(\text{hkl})_{\text{best}}| / |F(\text{hkl})|$; $F(\text{hkl})_{\text{best}} = S_{\alpha} P(\alpha) F_{\text{hkl}}(\alpha) / S_{\alpha} P(\alpha)$.^e $R = \sum_{\text{hkl}} |F_{\text{obs}}| - |F_{\text{calc}}| / \sum_{\text{hkl}} |F_{\text{obs}}|$; R_{work} , $\text{hkl} \notin T$; R_{free} , $\text{hkl} \in T$; *T*, test set.^f Calculated with MolProbity (58).

exclusively involve residues from domain 2. The PLP phosphate group is positioned over the N terminus of helix $\alpha 5$, interacting favorably with the helix macro-dipole and engaging in hydrogen bonds to the backbone amides of Thr-144 and Gly-145. The pyridine nitrogen maintains hydrogen bonds to the side chains of Cys-175 and Asn-252. Asn-252 is

at variance with the vast majority of fold type I enzymes, in which an Asp at the equivalent position is the only strictly conserved residue apart from the PLP-bound Lys (40). An Asn is expected to support the electron sink character of the pyridine ring less than an Asp, possibly demanding a good leaving group such as a phosphate on the β -carbon. Interest-

FIGURE 2. **Structure-based multiple sequence alignment of SecS and enzymes of the fold type I family.** Structure-based multiple sequence alignment generated by the 3DCoffee-option of Toffee (57) and shaded by BoxShade. Sequences are numbered at the beginning of each line. The darker background represents higher conservation. The background of the PLP lysines is in gold; the background of residues whose side chains contact PLP and of residues contacting the P1 phosphate is in green. P-loop residues undergoing a disorder-order transition upon phosphate binding are boxed in red. Residues contacting the P2 phosphate are indicated by a green arrowhead. Elements I–IV discussed in the text are indicated by labeled red bars above the alignment (see also Fig. 3). Active site loops 1 and 2 from element II are indicated by dashed lines below the alignment. Secondary structure elements as found in *mmuSecS*^{elast} are indicated below the alignment. Scaffolding elements are color-coded by domain; blue, domain 1; cyan, domain 2; steel blue, domain 3. Secondary structure elements belonging to elements I–IV are in red, and helix $\alpha 10$ (bearing the PLP cofactor) is in gold. *hsa*, *Homo sapiens*; *mmu*, *Mus musculus*; *dme*, *Drosophila melanogaster*; *cel*, *Caenorhabditis elegans*; *mma*, *Methanococcus maripaludis*; *mja*, *M. jannaschii*; *afu*, *A. fulgidus*; *syn*, *Synechocystis*; *eco*, *E. coli*; *tma*, *T. maritima*.

Structure and Mechanism of Eukaryotic Selenocysteine Synthase

TABLE 2

Structural comparison of three fold type I PLP-dependent enzymes with *mmuSecS^{elast}*

r.m.s.d., root mean square deviation.

	<i>afuPserCysS</i>	<i>tmaNifS</i> -like Protein	<i>synC-DES</i>
PDB code	2E7J	1EG5	1ELU
Reference	41	43	47
Sequence identity (%)	10.9	13.1	11.7
Matching C α atoms	257	283	266
r.m.s.d. (Å) ^a	2.8	2.8	3.0

^a Structures were superimposed by secondary structure matching (59).

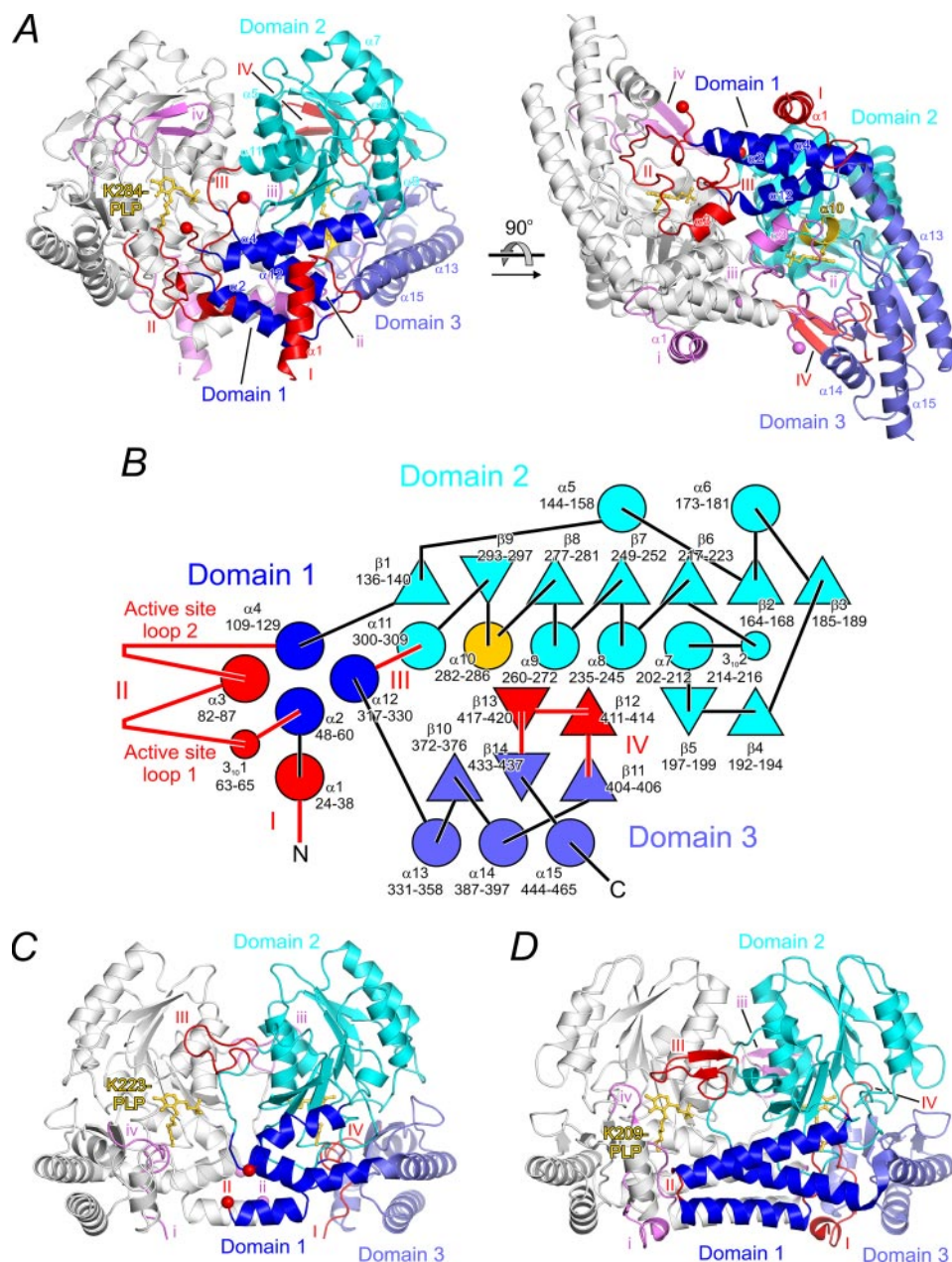


FIGURE 3. Domain organization and functional elements. *A*, orthogonal ribbon plots (front and bottom) of *mmuSecS^{elast}*. One protomer is in light gray, and the other protomer is color-coded according to domains (blue, scaffold of domain 1; cyan, scaffold of domain 2; steel blue, scaffold of domain 3). Selected elements (I–IV) as discussed in the text are shown in red and labeled with uppercase roman numerals for the reference molecule (*Mol I*) viz. in violet and labeled with lowercase roman numerals for the other protomer (*Mol II*). Helix $\alpha 7$, bearing the PLP cofactor, is in gold. Selected α -helices are labeled as landmarks. *B*, secondary structure topology (large circles, α -helices; small circles, 3_{10} -helices; triangles, β -strands). The secondary structure elements are labeled, and their residue extents are indicated. They are colored as in *A*. *C* and *D*, ribbon diagrams of *afuPserCysS* (*C*, PDB code 2E7J (41)) and *synC-DES* (*D*, PDB code 1ELU; (47)) dimers in the front view after global superimposition of the proteins on *mmuSecS^{elast}*. Coloring is the same as for *mmuSecS^{elast}*.

ingly, in *afuPserCysS*, in which phosphate is also the leaving group, the pyridine nitrogen is again bound to an Asn (Fig. 2) (41). The PLP pyridine ring of *mmuSecS^{elast}* is sandwiched between the side chains of Gln-172 and Ala-254 on the re and si faces, respectively. Archaeal SecS enzymes feature a His in place of Gln-172 (Fig. 2). A similar His in a NifS-like protein from *Thermotoga maritima* has been discussed as a tunable acid-base catalyst in the reaction mechanism (43). Thus, the enzymatic mechanisms of archaeal and eukaryotic

SecS may differ in detail.

Interactions with PLP in *trans* (Fig. 4, *A* and *B*) involve residues from the SecS-specific insertion in domain 1 (element II) and from the short element III connecting domain 2 and the second part of domain 1 (Fig. 3, *A* and *B*). Both elements primarily interact with the PLP phosphate. Arg-75 (originating from the first loop of element II) is deposited on the phosphate side of the PLP pyridine ring where its side chain can engage in two charged interactions with anionic phosphate oxygens. Arg-75 is appropriately positioned by a double salt bridge interaction with Asp-283 from the cis protomer (Fig. 4, *A* and *B*). The preceding residue of element II, Glu-74, comes to lie on the opposite side of the pyridine ring and is connected via water molecules to the C3 hydroxyl group of PLP and the nitrogen of the Schiff base. It is kept in place by van der Waals contacts to Tyr-255 of the cis protomer (Fig. 4, *A* and *B*). In addition, the backbone nitrogen of Arg-313 (from element III) hydrogen bonds to an anionic phosphate oxygen of the PLP.

In other fold type I PLP-dependent enzymes, element III is often significantly longer than in SecS (Fig. 3, *C* and *D*) and provides additional residues for binding the PLP phosphate. In contrast, the region corresponding to element II in *afuPserCysS* is much shorter than in SecS (21 versus 47 residues) and is completely disordered in the structure (41), failing to provide stable PLP anchoring (Fig. 3*C*). In *synC-DES*, the equivalents of helices $\alpha 2$ and $\alpha 4$ are longer and place a very short element II, which is suspended between them, remote from the *trans* PLP and close to domain 3

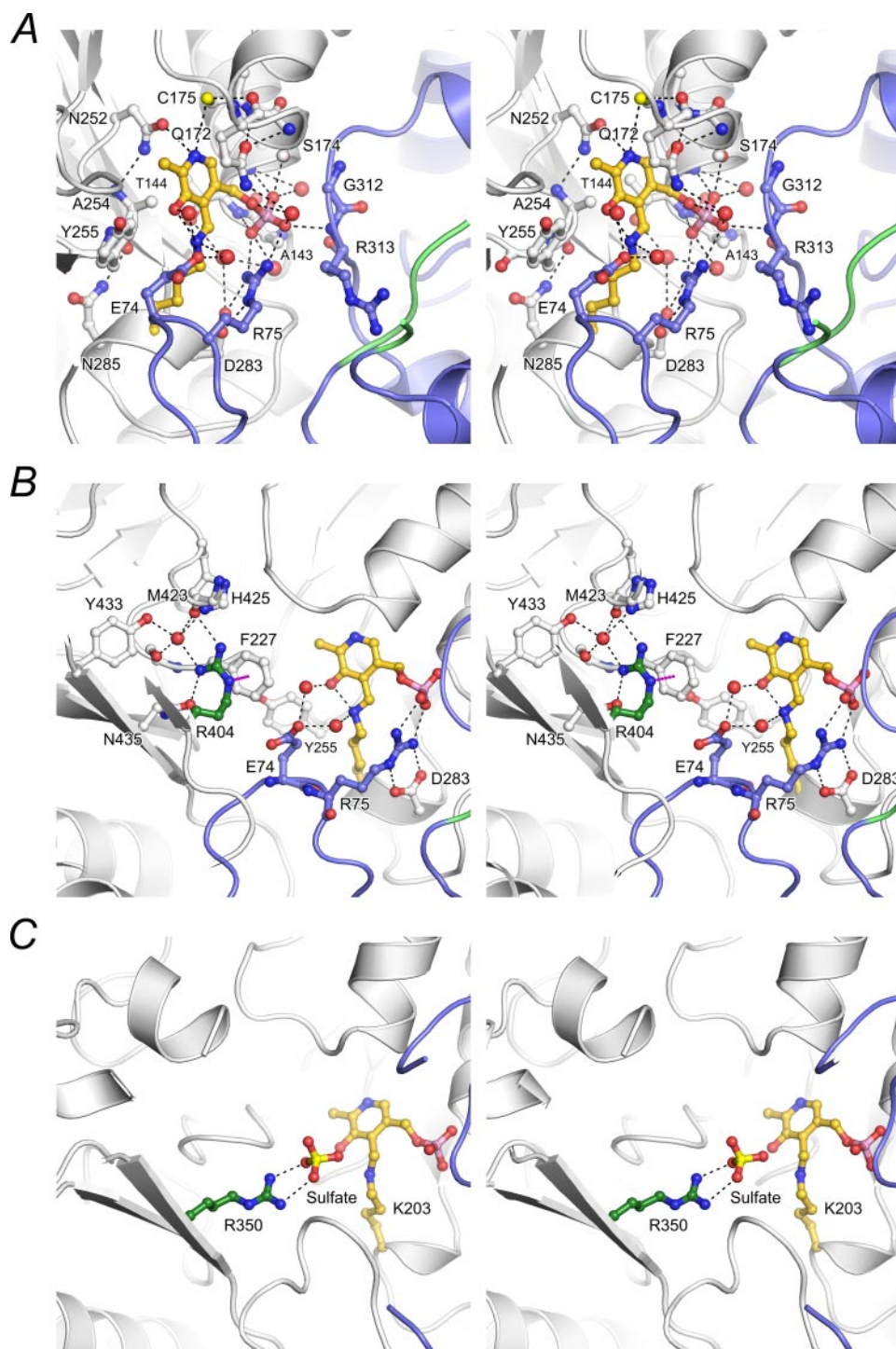
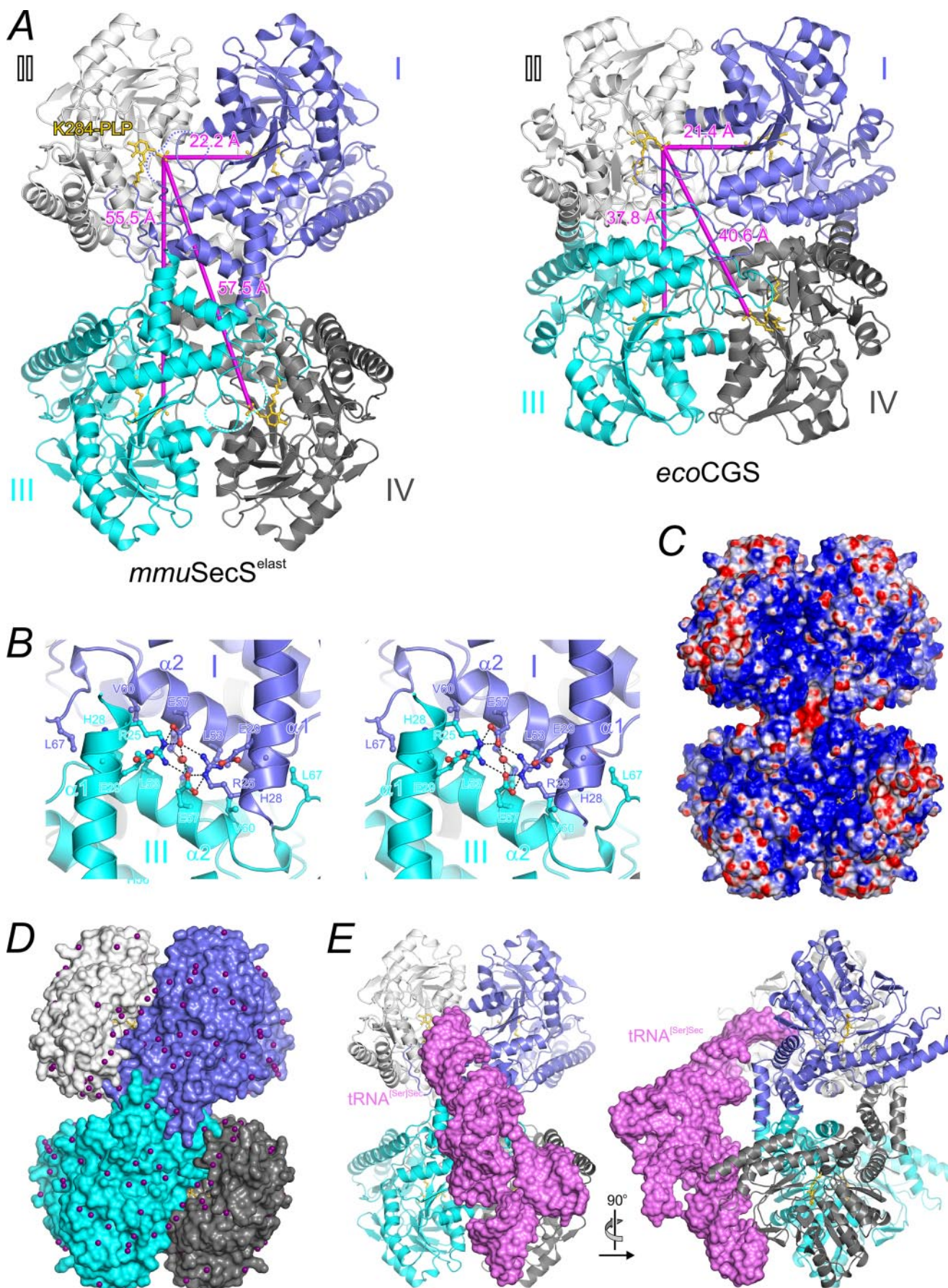


FIGURE 4. PLP environment. **A**, stereo ribbon plot depicting the anchoring of PLP by two protomers of a close dimer in native *mmuSecS*^{elast}. The backbone of the molecule binding PLP in cis is shown in light gray, and the backbone of the molecule binding in trans is in steel blue. The base of the disordered loop (P-loop; see also Fig. 6) is in green. The Lys-284-bound PLP and selected residues from both protomers are shown in ball-and-stick representation and are color-coded by atom type (carbon, as the respective protein backbone; gold, carbon of Lys-284-PLP; blue, nitrogen; red, oxygen; yellow, sulfur; pink, phosphorus). Red spheres designate water molecules. Dashed lines indicate hydrogen bonds and salt bridges. The view is rotated 30° about the vertical axis compared with the front view in Fig. 3A. **B**, stereo ribbon plot of the remodeled neighborhood of PLP. Selected residues are shown in ball-and-stick representations. Green, carbon of Arg-404. Other colors are as in A. Black dashed lines indicate hydrogen bonds and salt bridges. The magenta dashed line shows a cation- π stack of the side chains of Arg-404 on Phe-227. The view is rotated 90° about the vertical axis compared with the front view in Fig. 3A. **C**, stereo ribbon plot of the PLP neighborhood in a *T. maritima* NifS-like protein (PDB code 1EG5 (43)) after global superimposition on *mmuSecS*^{elast}. The view and color-coding are the same as in panel B. Arg-350 of *T. maritima* NifS is the equivalent of Arg-404 in *mmuSecS*^{elast}. In the absence of a substrate it binds to a sulfate ion mimicking a α -carboxylate.

of the other protomer (Fig. 3D). Thus, in other fold type I enzymes, element II serves to reinforce dimerization but does not contribute directly to the active sites. Instead, in *afuP*SerCysS, NifS relatives and *synC*-DES a portion of the N terminus is positioned between domains 1 and 3 and harbors residues, which in some cases contact the cis PLP (Fig. 3, C and D). In *mmuSecS*^{elast}, the first loop of the long element II replaces this N-terminal part in trans (Fig. 3A).

In contrast to the situation within a close dimer, there is no cross-communication at the active sites between molecules belonging to the two different close dimers of a tetramer. This situation suggests that the close dimers are sufficient to provide the chemical microenvironment required for catalysis.

Binding of Phosphate Triggers Disorder-Order Transition in an Active Site Loop—Substrates of SecS contain a number of phosphates or phosphate-related groups, such as the phosphodiester backbone of tRNA^{[Ser]Sec}, the γ -phosphate of the PSer moiety, and SeP. We reasoned that phosphate could mimic binding of either of these groups at the active site of SecS and determined the crystal structure of *mmuSecS*^{elast} after soaking crystals for 30 s in 0.5 M phosphate buffer. Strikingly, we observed that a phosphate (P1 in Fig. 6) is cradled in the second loop of the domain 1 insertion (residues 98–104 of element II; green in Fig. 6), which was previously disordered. Upon phosphate binding, this loop contracts and covers part of the trans active site (Fig. 6, A and B). Arg-313 originating from the loop that connects domain 2 to the second part of domain 1 (element III in Fig. 3, A and B) forms the base of the P1 phosphate binding site. To bind the P1 phosphate, Arg-313 and Gln-105 (neighboring the previously disordered element) are profoundly repositioned (Fig. 6, C and D). In addition, the P1 phosphate interacts directly as well as via a water bridge with the side chain of Arg-97 and with the side chain and backbone of



Ser-98, both of which were disordered in the absence of phosphate (Fig. 6, C and D).

A poly-dentate anion appears to be required to engage in the observed interactions and elicit the structural transition. In agreement with this notion, a similar disorder-order transition was observed upon soaking with sulfate ions (not shown), whereas mono-dentate anions did not evoke any such change. For example, 250 mM NaCl were present in all crystallization and soaking experiments, and we did not observe any conformational changes in the structure soaked with an additional 0.5 M sodium iodide (Table 1). We, therefore, refer to the loop between Gly-96 and Pro-106 of element II as the “phosphate loop” (P-loop).

Upon binding of the P1 phosphate, the P-loop closes off part of the active site of *mmuSecS*^{elast} (Fig. 6, A and B). It is likely that active site closure accompanies catalysis and may serve, e.g. to locally exclude bulk water. Therefore, the 3'-end of tRNA^{[Ser]Sec} most likely gains access to the PLP cofactor from the side opposite the P-loop (arrow in Fig. 6B).

We observed a second phosphate binding site remote from the active site (P2 in Fig. 6B). This phosphate location could indicate a site of contact to the tRNA^{[Ser]Sec} phosphodiester backbone. However, in contrast to the P-loop and Arg-313 (see below), residues contacting the P2 phosphate (Arg-199, His-368) are not conserved in SecS orthologs (Fig. 2). It is possible that the binding of the P2 phosphate is not functional and restricted to mouse and a few other SecSs.

Phosphate Binding Is Mediated by Conserved and SecS-specific Residues That Are Essential for Selenocysteine Synthesis—The P-loop is a highly conserved element of eukaryotic and archaeal SecS, which is lacking from related enzymes with a different function (Fig. 2). In particular, Arg-97, Ser-98, and Gln-105 from the P-loop as well as Arg-313 from element III, which directly contact the P1 phosphate, are strictly conserved among SecS enzymes but not beyond. These observations are consistent with the idea that the P-loop carries out an essential function that is specific for SecSs.

To directly probe the importance of residues contacting the P1 phosphate, we generated mutant *mmuSecS* proteins in which Gln-105 was changed to Glu (*mmuSecS*^{Q105E}) or Arg-313 was changed to Ser or Glu (*mmuSecS*^{R313S}; *mmuSecS*^{R313E}). All mutants were expressed as soluble proteins in *E. coli*, migrated as tetramers in gel filtration, and exhibited a PLP complement comparable with that of the wild type protein, as indicated by their absorption maxima at 334 nm (ketimine form) and 418 nm (aldimine form; not shown). We tested the mutants for their ability to convert PSer-tRNA^{[Ser]Sec} to Sec-tRNA^{[Ser]Sec}. Strikingly, each of the point mutants severely corrupted the activity of *mmuSecS* (Fig. 7A). Although the *mmuSecS*^{Q105E} and *mmuSecS*^{R313S} mutants still exhibited

activities of about 50 and 30% of the wild type protein, respectively, the R313E exchange rendered *mmuSecS* virtually inactive (Fig. 7A). The more severe effect with the negatively charged Glu compared with the neutral Ser in place of Arg-313 directly supports the functional relevance of phosphate binding at this position. These results directly link the ability of *mmuSecS* to bind a phosphate or a related group via induced fit of the P-loop to its catalytic competence. Based on these observations, we suggest that the P1 phosphate mimics binding of a substrate or of a functional portion of a substrate.

The P-loop Could Serve as a Binding Site for the PSer γ -Phosphate and SeP—We scrutinized the possibility that the γ -phosphate of PSer-tRNA^{[Ser]Sec} could be bound by the P-loop. To this end we modeled the structure of an external aldimine comprising PLP in a Schiff-base linkage to a PSer esterified at the α -carboxylate. For modeling, we superimposed the structure of PSer-aminotransferase in complex with the substrate mimic α -methyl-L-glutamate (49) onto the *mmuSecS*^{elast}-phosphate structure. We replaced the α -methyl-L-glutamate moiety with a α -carboxy ester of PSer, retained all side chain conformations as observed in the *mmuSecS*^{elast} structure in complex with phosphate, and allowed the PLP moiety to adopt a slightly more inclined orientation (Fig. 6E). Even without adjustments of the protein matrix, the γ -phosphate of the PSer ester could be accommodated approximately at the P1 phosphate position. These results suggest that the P-loop could serve to bind the γ -phosphate of PSer-tRNA^{[Ser]Sec}.

The similarity of phosphate and SeP suggests that the P1 phosphate could also mimic binding of the co-substrate SeP to the P-loop. Binding of the PSer moiety and SeP to the P-loop could occur sequentially and is not mutually exclusive (see “Discussion”). In contrast, we did not manage to fit a phosphate from the backbone of tRNA^{[Ser]Sec} without clashes in the position of the P1 phosphate at the P-loop, consistent with our above suggestion that the tRNA^{[Ser]Sec} 3'-end approaches the active site distal to the P-loop (Fig. 6B).

SecS Discriminates against Free O-Phospho-L-serine—Free PSer is produced, for example, as an intermediate in the biosynthesis of serine by transamination from 3-phosphohydroxypyruvate. Therefore, SecS should be safeguarded against using free PSer as a substrate. We tested this notion by attempting to dephosphorylate free PSer with *mmuSecS*. Indeed, the enzyme proved to be completely unreactive with respect to the free amino acid (Fig. 7B).

We inspected the active site of *mmuSecS*^{elast} for possible filtering devices. Typically, PLP-dependent enzymes of the fold type I deploy a positively charged Arg in the neighborhood of the PLP to bind the negatively charged α -carboxylate of an amino acid substrate. In the absence of a substrate, a sulfate or phosphate group often binds at an equivalent position as the

FIGURE 5. **The *mmuSecS*^{elast} tetramer.** A, left, overview of the *mmuSecS*^{elast} homotetramer, comprising a dimer of dimers (222 symmetry). Protomers (*MolI*–*IV*) are shown in different colors. Distances between active sites (PLP phosphates) are indicated (magenta lines). Right, overview of the *E. coli* cystathionine γ -synthase (*ecoCGS*) homotetramer (PDB code 1CS1 (55)) drawn to scale and in the same orientation as the *mmuSecS*^{elast} tetramer. B, stereo ribbon plot of the N-terminal tetramerization motif. Selected residues are shown as ball-and-stick representations and color-coded by atom type. Dashed lines indicate hydrogen bonds and salt bridges. C, electrostatic surface potential of the tetramer (calculated with PLP omitted). Blue, positive charge; red, negative charge. Large positively charged patches, in particular around the active site funnel, can be discerned. Lys-284-bound PLP moieties are shown in gold at the bottom of the active sites funnels. D, iodide ions (purple spheres) located in the structure of *mmuSecS*^{elast} soaked in 0.5 M sodium iodide. E, hypothetical model of tRNA^{[Ser]Sec} binding to *mmuSecS*^{elast}. No local conformational adjustments or energy minimizations were conducted in either the protein or the tRNA to optimize the fit.

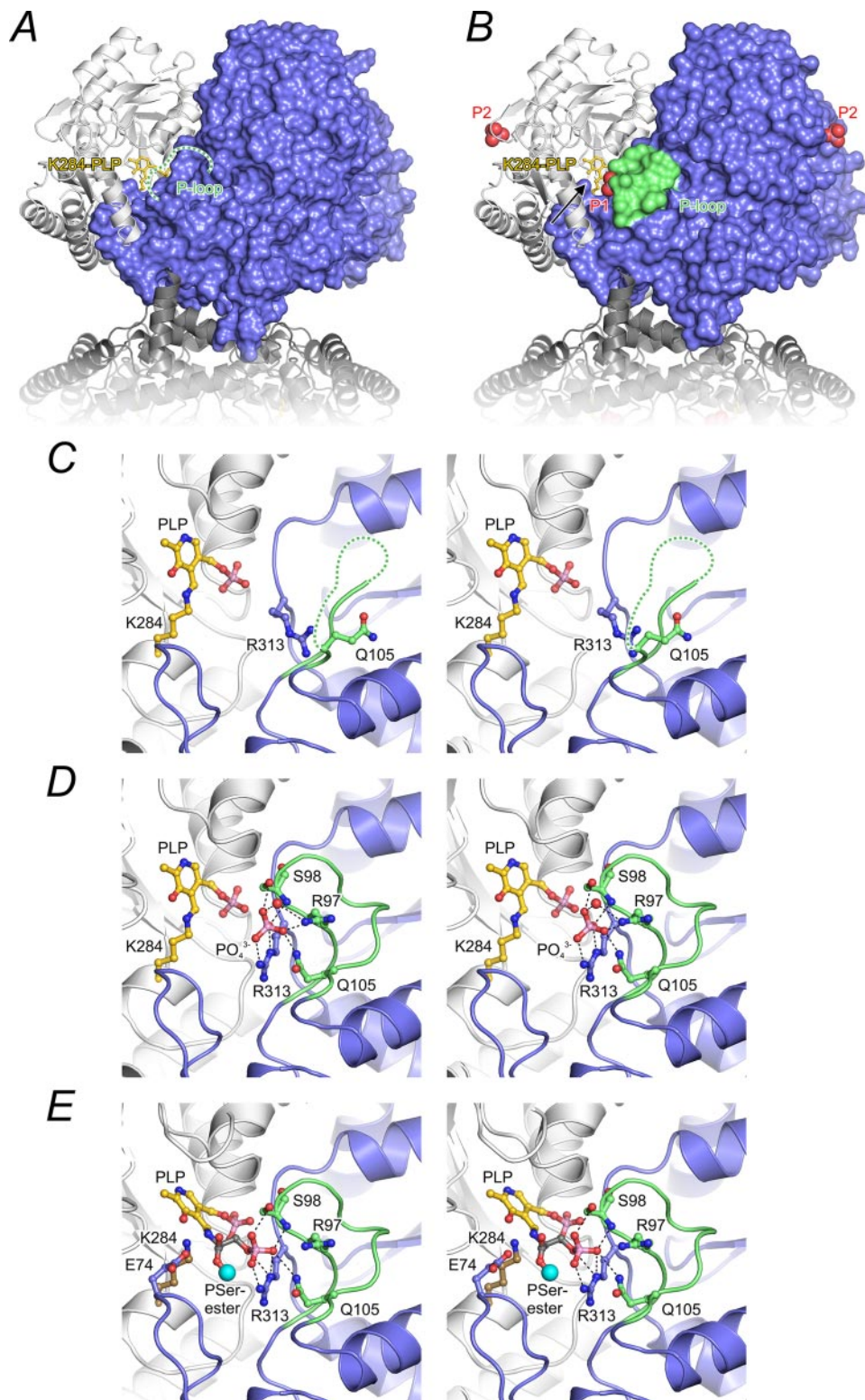
Structure and Mechanism of Eukaryotic Selenocysteine Synthase

α -carboxylate (43). The α -carboxylate binding Arg originates in cis from the β -sheet in domain 3. An equivalent Arg is also strictly conserved in SecS orthologs (Arg-404; Fig. 4B). However, in *mmu*SecS^{elast}, its side chain is turned away from the PLP. Arg-404 interacts instead by a cation- π interaction with Phe227 (another residue strictly conserved only in the SecS orthologs; Fig. 2). It is additionally fixed by hydrogen bonds to the side chain of Asn-435 and the backbone carbonyl of Met-423 and by water-mediated hydrogen bonds to the backbone carbonyl of Ala-228 and to side chains of His-425 and Tyr-433 (Fig. 4B). The side chain of Arg-404 is thereby stably tugged away, since it does not change orientation in the presence of even 0.5 M phosphate (as seen in our phosphate-soaked structure), suggesting that Arg-404 is not involved in binding of a α -carboxylate.

As pointed out above, *mmu*SecS^{elast} harbors Glu-74 in trans next to the PLP moiety (Fig. 4, A and B). Interestingly, Glu-74 occupies the same spatial position as the equivalent of Arg-404 in other fold type I enzymes (Fig. 4, B and C). This observation and our model of an external aldimine of *mmu*SecS with a PSer ester (Fig. 6E) demonstrate that Glu-74 would strongly disfavor productive placement of a substrate with a free (negatively charged) α -carboxylate. In PSer-tRNA^[Ser]Sec, however, the α -carboxylate of PSer is esterified to the 2'- or 3'-hydroxyl group of the 3'-terminal adenosine and does not carry a negative charge. Therefore, we expect that Glu-74 acts as a substrate filter by repelling compounds with a negatively charged α -carboxylate.

The Inhibition Profile of SecS Resembles That of β -Lyases—To gain additional insight into the reaction mechanism of SecS, we tested whether the dephosphorylation activity of *mmu*SecS is inhibited by the mechanism-based inhibitors PG and F₃-Ala. PG preferentially inhibits PLP-dependent enzymes such as cystathionine γ -lyase, which mediate lyase reactions at the γ -carbon (50). In contrast, F₃-Ala preferentially inhibits enzymes such as cystathionine β -lyase, which mediate replacement of a substituent at the β -car-

bon (51). Strikingly, *mmu*SecS is unaffected by up to 25 mM PG (more than 12,500-fold excess over *mmu*SecS active sites; Fig. 7C). In contrast, partial enzyme inhibition was detected in the presence of 5 mM F₃-Ala and above (Fig. 7C). These inhibition profiles are in agreement with SecS catalyzing a β -replacement reaction with a high specificity. Furthermore, the data suggest that the lytic half-reaction of SecS



follows the cystathionine β -lyase scheme, strongly supporting aminoacyl-tRNA^{[Ser]^{Sec}} as an intermediate (28).

Although our data do not allow us to derive exact inhibition constants, we note that compared with *E. coli* cystathionine β -lyase (51), the inhibition of *mmu*SecS by F₃-Ala is weak. For example, in a comparable setup, the half-time for inactivation of *E. coli* cystathionine β -lyase by 1 mM F₃-Ala was less than 2 min (52), whereas *mmu*SecS is not measurably affected under these conditions (Fig. 7C). This observation is consistent with the suggested substrate discrimination by Glu-74, since F₃-Ala exhibits a free α -carboxylate and is, therefore, expected to be discouraged from forming an external aldimine.

DISCUSSION

SecS Orthologs Constitute a Unique Subclass of Fold Type I PLP-dependent Enzymes—We have presented structural and functional analyses of a mammalian SecS demonstrating how SecS orthologs are set aside from other PLP-dependent enzymes. Although *mmu*SecS^{elast} is composed of three domains whose structural scaffolds exhibit high similarity to the fold type I family of PLP-dependent enzymes (Fig. 3), distinguishing structural and functional characteristics are conferred by remodeled elements both within and outside of these conserved scaffolds (labeled I–IV in Fig. 3). These novel elements clearly define SecS orthologs as a special subclass of the family.

Of paramount importance for the function of SecS are two motifs that are unique to and highly conserved in SecS orthologs. First, a special N terminus (element I) serves as a tetramerization device. It reinforces the interaction between two close dimers by cross-strutting (Fig. 5, A and B). Neither *afu*PserCysS nor NifS relatives nor *synC*-DES exhibit a comparable element, and all of these enzymes form dimers. As further detailed below, we suggest that tetramerization could be crucial for proper Pser-tRNA^{[Ser]^{Sec}} positioning. Second, a long insertion between helices α 2 and α 4 of domain 1 (element II) is involved in catalysis by SecS. Via a first loop, element II provides residues Glu-74 and Arg-75, which anchor the PLP cofactor in trans. It thereby positions the negatively charged Glu-74 ideally to act as a substrate filter. Via a second loop it dispatches the P-loop to the trans active site, which mediates binding of SecS-specific substrates.

Evidently, the evolution of the unique N terminus and of the long domain 1 insertion went hand in hand. Placing the N terminus at the outside of the protein, where it can engage in tetramer formation, liberated a binding site between domains 1

and 3 as seen, e.g. in *afu*PserCysS, NifS relatives, and *synC*-DES proteins (Fig. 3). The first loop of the domain 1 insertion evolved to take advantage of the liberated binding site between domains 1 and 3 in trans. It thereby became ideally positioned to contribute residues to the trans active site (Fig. 3A).

tRNA Selection Strategy of SecS—Our results highlight a number of features that enable SecS to specifically recognize its substrates. The highly positively charged surface of *mmu*SecS^{elast} is apparently designed to interact at multiple sites with the phosphodiester backbone of tRNA^{[Ser]^{Sec}}. This expected mode of interaction is supported by our observations of numerous anion (iodide) binding sites (Fig. 5D), binding of a chloride ion in untreated crystals (not shown), and binding of the P2 phosphate ion distal to the active sites in phosphate-soaked crystals (Fig. 6B). tRNA^{[Ser]^{Sec}} exhibits a number of unique structural characteristics compared with canonical tRNAs, such as an elongated (9 + 4 base pairs) helical stack between the acceptor stem and the T Ψ C stem and an unusually long variable arm (8, 53). Multiple latching points on the surface of SecS would allow the enzyme to recognize these global structural features and discriminate against other tRNAs, which are in vast excess in the cell. Thus, the tRNA selection strategy of SecS may resemble that of bacterial SelA, which very inefficiently converts Ser-tRNA^{[Ser]^{Sec}} mutants with a shortened, canonical acceptor stem (54).

The *mmu*SecS^{elast} active site environments are built up entirely by residues originating from the two protomers of a close dimer. Why then does *mmu*SecS form tetramers? One possibility is that the tetramer provides an effective binding platform for the large tRNA^{[Ser]^{Sec}} molecule. Although we have no direct evidence for the mode of Pser-tRNA^{[Ser]^{Sec}} binding to *mmu*SecS, portions of tRNA^{[Ser]^{Sec}} could extend beyond the borders of the molecule to whose active site its 3'-end is bound. To illustrate the relative sizes of the molecules and how the SecS tetramer could serve as a binding platform for tRNA^{[Ser]^{Sec}}, we generated a hypothetical docking model (Fig. 5E). A model of tRNA^{[Ser]^{Sec}} (as derived in Hubert *et al.* (53)) was positioned on the *mmu*SecS^{elast} tetramer with the 3'-end approaching the active site of one monomer distal to the P-loop, leaving the P-loop available for accommodation of the Pser moiety. The body of tRNA^{[Ser]^{Sec}} was then adjusted by rotation about the 3'-terminal nucleotide to avoid clashes with the protein. Significantly, the unique mode of tetramerization provides the *mmu*SecS tetramer with a unique, elongated shape (shown by the characteristic distances between the active sites;

FIGURE 6. Phosphate-induced conformational changes. A, native *mmu*SecS^{elast} close dimer with one molecule shown as a light gray ribbon and the other as a blue surface; the other protomers of the tetramer are shown as gray ribbons fading out. Residues 98–104 (dashed line) of the P-loop (green) are completely disordered. A Lys-284-bound PLP is shown in gold ball-and-stick representation. The view is the same as in Fig. 3A. B, upon binding of the P1 phosphate, the previously disordered region of the P-loop becomes completely ordered and closes part of the active site like a lid (green surface). Bound phosphates are shown as space-filling models (red, oxygen; pink, phosphorus). The P2 phosphate may indicate a distal site of attachment of a portion of the tRNA^{[Ser]^{Sec}} backbone. The arrow indicates the likely access path of the tRNA^{[Ser]^{Sec}} 3'-end. C, stereo ribbon plot of the active site formed around the Lys-284-bound PLP of a reference molecule (light gray backbone) with participation by the second protomer of the close dimer (steel blue backbone). The partially disordered (dashed line) flexible P-loop of the second molecule is shown in green. The Lys-284-bound PLP and selected residues are shown as ball-and-stick representations and are color-coded by atom type as before. Note that the side chains of Gln-105 and Arg-313 are turned away from the Lys-284-PLP moiety. The view is rotated 30° around the vertical axis compared with the views in panels A and B. D, stereo ribbon plot of the same active site region after binding of the P1 phosphate. Gln-105 and Arg-313 change their positions and orientations drastically to engage in hydrogen bonds *viz.* salt bridges to the phosphate oxygens. In addition, residues Arg-97 and Ser-98 of the P-loop engage in phosphate binding, leading to a complete ordering of the P-loop. Orientation and color-coding are as in panel C. Dashed lines indicate salt bridges and hydrogen bonds. E, model for binding of Pser esterified at the α -carboxyl (cyan sphere). Without major adjustments of the protein matrix, the γ -phosphate can be cradled in the P-loop similar to the free phosphate in D. Note that Glu-74 closely approaches the α -carboxy ester.

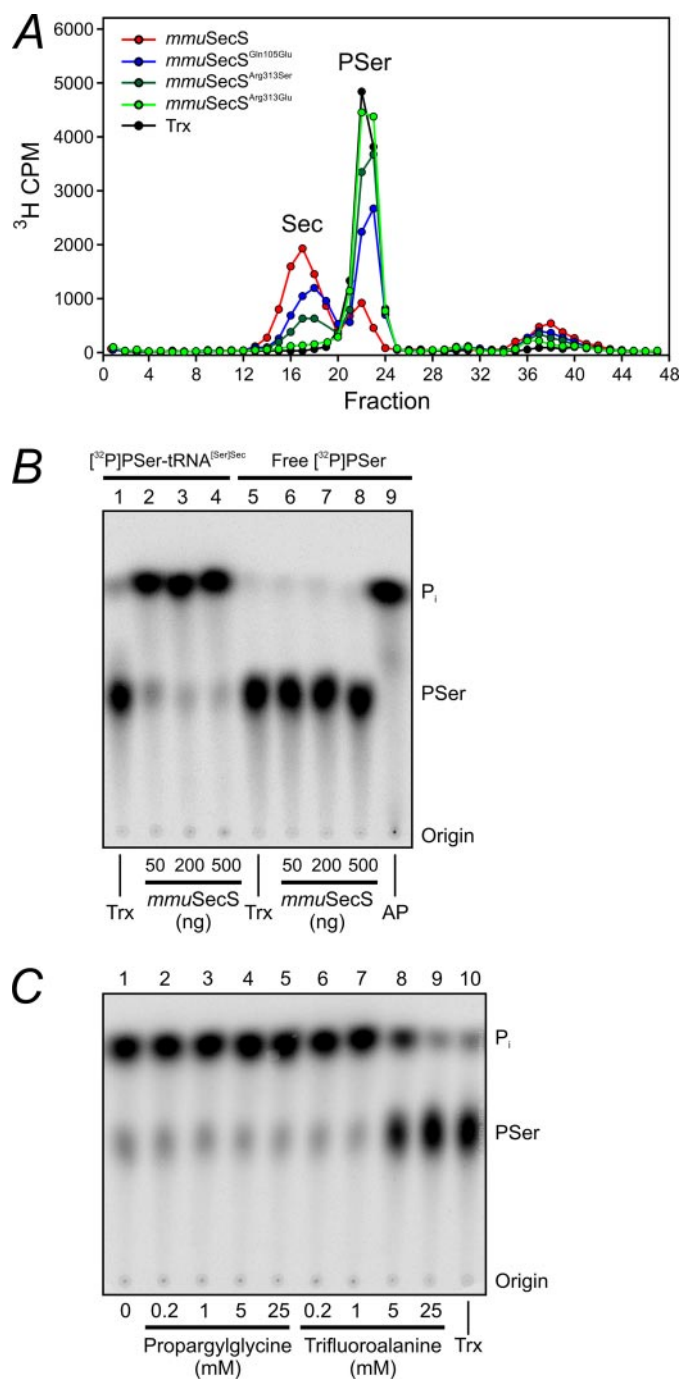


FIGURE 7. Functional analysis of *mmuSecS*. A, mutational analysis of *mmuSecS*. Conversion of [^3H]Pser-tRNA^{[Ser]Sec} to [^3H]Sec-tRNA^{[Ser]Sec} by *mmuSecS* (red), *mmuSecS*^{Q105E} (blue), *mmuSecS*^{R313S} (dark green), and *mmuSecS*^{R313E} (light green). Trx (black) served as a negative control. B, dephosphorylation activity of *mmuSecS*. Dephosphorylation of [^{32}P]Pser-tRNA^{[Ser]Sec} (lanes 1–4) and [^{32}P]Pser (lanes 5–9) in the presence of varying amounts of *mmuSecS* is shown. Trx was used as a negative control (lanes 1 and 5), and alkaline phosphatase (AP) was used as a positive control for the generation of free [^{32}P]P_i (lane 9). Details are given under “Experimental Procedures.” C, inhibition studies of *mmuSecS*. [^{32}P]Pser-tRNA^{[Ser]Sec} dephosphorylation with *mmuSecS* (lane 1) in the presence of the mechanism-based inhibitors PG (lanes 2–5) and F₃-Ala (lanes 6–9). Trx (lane 10) served as a negative control. Details of reactions and monitoring conditions are given under “Experimental Procedures.”

Fig. 5A). Other arrangements, such as the stubbier form of *E. coli* cystathionine γ -synthase (Fig. 5A) (55), generate other relative dispositions of active sites. Thus, SecS may have

evolved as a distinctly shaped tetramer to support efficient Pser-tRNA^{[Ser]Sec} binding by one dimer to position its 3'-end appropriately in an active site of a neighboring dimer. A similar principle may underlie the decameric organization of bacterial Sela. Further experiments are required to test these ideas.

Mechanisms for Substrate Binding and Differentiation in the Active Site—Our structural analyses have shown that the long, conserved domain 1 insertion (element II) of *mmuSecS* does not merely serve to support PLP anchoring in trans. Part of this insertion, which we refer to as the P-loop, can undergo disorder-order transitions coupled to binding of poly-dentate ions such as phosphate or sulfate. We interpret this observation as direct evidence for the mode of substrate binding by *mmuSecS*. Our molecular modeling suggests that the P1 phosphate could resemble the binding of the γ -phosphate of the Pser moiety of Pser-tRNA^{[Ser]Sec} (Fig. 6E). Evidently, SeP could also bind to the P-loop in a similar fashion as the P1 phosphate. In contrast, we could not position the tRNA^{[Ser]Sec} phosphodiester backbone in the same way at the P-loop. In any case, the P-loop in combination with Arg-313 (from element III) obviously binds and positions phosphate portions of substrates by an induced fit mechanism. This notion is perfectly borne out by our mutational analyses, which showed that the phosphate-coordinating residues are crucial for *mmuSecS* activity (Fig. 7A).

In addition, we suggest that SecS has exploited the domain 1 insertion to install a filtering mechanism that allows it to exclude free Pser and other free amino acids from its active site. Glu-74, positioned strategically next to the trans PLP (Fig. 4, A and B), adopts a similar spatial position as the side chain of an Arg originating from the domain 3 β -sheet in related enzymes, which typically serves as an α -carboxylate recognition device (Fig. 4C). In SecS, an equivalent Arg is present, but it is turned away via interactions with other conserved residues (Fig. 4B), e.g. to engage in alternative interactions with the tRNA^{[Ser]Sec} portion. We suspect that Glu-74 repels negatively charged carboxyl groups of free amino acids. Neutral ester moieties as in Pser-tRNA^{[Ser]Sec} are presumably allowed to productively approach the PLP internal aldimine. Our finding that SecS does not convert free Pser supports the role of Glu-74 as a substrate discriminator. Similar to the P-loop, the elements constituting the putative substrate filter are highly conserved among SecS orthologs but not beyond. Thus, SecS has acquired specialized functional modules for substrate binding and differentiation.

γ -Phosphate binding at the P-loop provides a facile explanation for the observation that SecS binds Pser-tRNA^{[Ser]Sec} preferentially over non-aminoacylated tRNA^{[Ser]Sec} (28). However, presently we can only speculate why Ser-tRNA^{[Ser]Sec} is bound with least efficiency (28). One clue is provided by the observations that the P-loop tends to bind substrate mimics such as phosphate or sulfate and that Pser-tRNA^{[Ser]Sec}, but not Ser-tRNA^{[Ser]Sec}, can compete efficiently with these molecules. The unloaded 3'-end of tRNA^{[Ser]Sec} may fit next to the contracted P-loop without having to compete for binding at that place. Another possibility is that γ -phosphate binding at the P-loop leads to proper accommodation of the Pser moiety and of the tRNA^{[Ser]Sec} 3'-end in the active site, whereas Ser at the 3'-end may engage in alternative interactions, which could be mutually exclusive with proper fitting of tRNA^{[Ser]Sec}. Clarification of

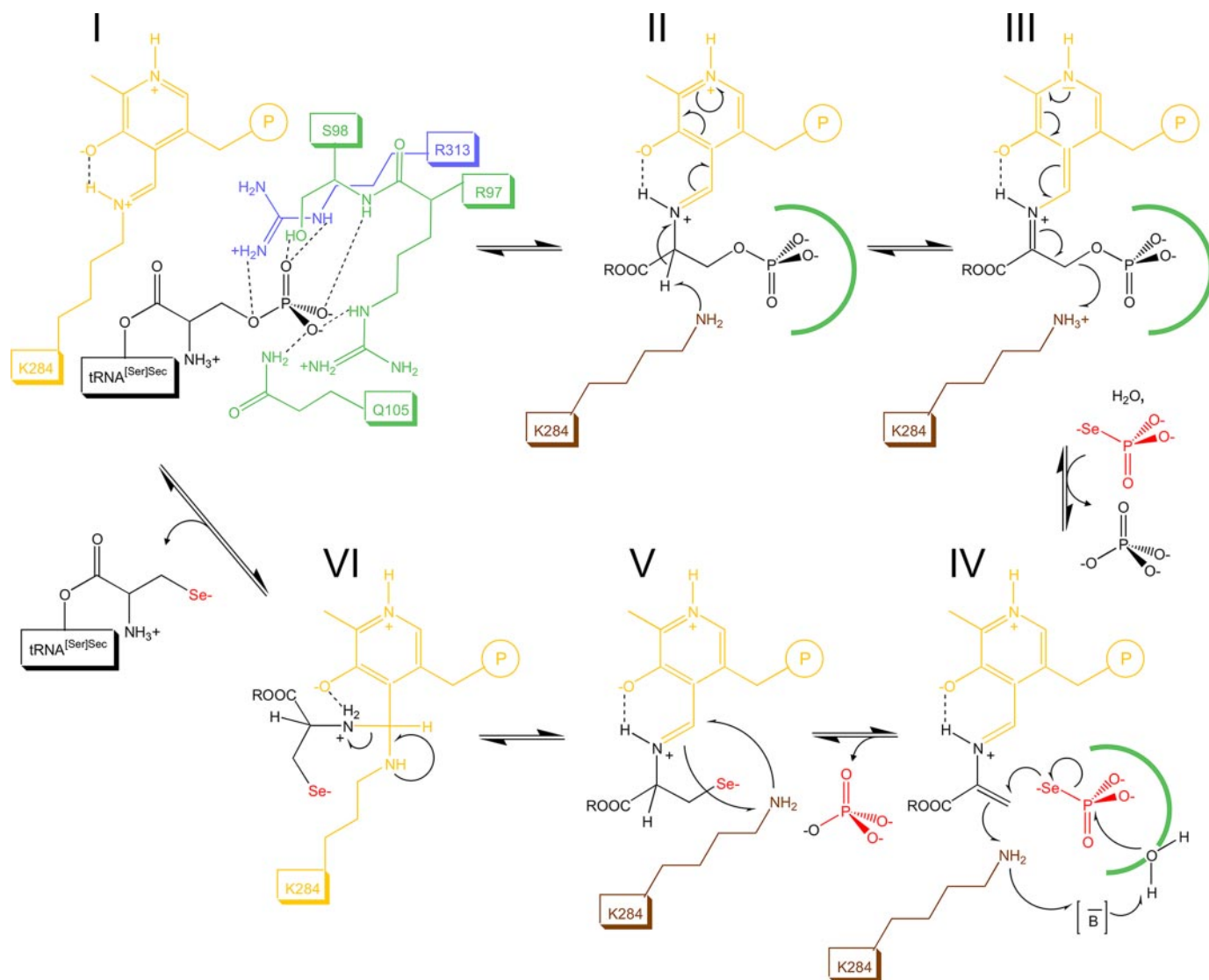


FIGURE 8. Proposed catalytic mechanism. Elements are color-coded: *gold*, PLP and the PLP-bound Lys-284; *brown*, liberated Lys-284; *green*, residues of the P-loop; *blue*, Arg-313; *black*, P-Ser-tRNA^{[Ser]Sec}; *red*, SeP. *R* in II–VI represents tRNA^{[Ser]Sec}. *I*, formation of the Michaelis complex, most likely involving binding of the γ -phosphate of P-Ser-tRNA^{[Ser]Sec} to the P-loop/Arg-313. In further steps, this binding site is symbolized by a *green arch*. *II*, abstraction of the α -proton from the internal aldimine by Lys-284. *III*, phosphate elimination and generation of aminoacrylyl-tRNA^{[Ser]Sec}; the evolving negative charge on the phosphate group is compensated by protonation via Lys-284. *IV*, SeP replaces phosphate at the P-loop/Arg-313 binding site. We suggest that attack of the aminoacrylyl-tRNA^{[Ser]Sec} intermediate by SeP involves concomitant attack by a water molecule on SeP. A general base (*B*) is proposed to activate this water molecule. Activation could be supported by a circular protonic shift involving Lys-284. *V* and *VI*, reverse transaldimination, regenerating the active site and release of the product, Sec-tRNA^{[Ser]Sec}. Further details are given under “Discussion.”.

these issues may require elucidation of a SecS-tRNA^{[Ser]Sec} complex structure.

Structure-based Reaction Mechanism—NifS-like enzymes mobilize sulfur for iron-sulfur cluster biosynthesis via a protein-bound persulfide using a conserved cysteine that lies in a long loop of domain 3 (element IV in Fig. 3, *A* and *B*) (43). *synC*-DES employs a related strategy by generating an external cysteine persulfide via cystine C-S cleavage, which remains non-covalently fixed at the active site (47). Furthermore, it has been discussed that P-Ser-CysS could also employ a persulfide mechanism (41). Because NifS can support selenide delivery (56), SecS could function in an analogous fashion by using a perselenide intermediate. However, although SecS exhibits a domain 3 loop analogous to the persulfide loop of NifS enzymes, no cysteine that could serve as attachment site for

selenium is present in that loop. The only cysteine that is conserved in eukaryotes in the active site cavity is Cys-226 (Fig. 2). However, its sulfur atom is still more than 7 Å away from any atom of the PLP and remote from the modeled substrate. In addition, this residue is not conserved in archaeal SecS (Fig. 2). Furthermore, in light of the observation that SeP delivered by selenophosphate synthetase 2 is the active selenium donor of SecS (24, 28), internal or external perselenide production (via SeP) appears to be an off-pathway reaction. Under these circumstances it is unlikely that SecS functions via an intermediate perselenide moiety.

Instead, a mechanism that is consistent with all our findings evokes direct selenide delivery by SeP (Fig. 8). As suggested by the inhibition results, we based the first part of the scheme on the *E. coli* cystathionine β -lyase mechanism (51). In our work-

ing model the process is initiated by P-Ser-tRNA^{[Ser]^{Sec} binding and positioning of the γ -phosphate at the P-loop (Fig. 8, I). Lys-284 is expected to be deprotonated after liberation upon external aldimine formation, constituting a strong base suitable for abstracting the α -hydrogen from the substrate (Fig. 8, II). Phosphate release would generate aminoacrylyl-tRNA^{[Ser]^{Sec} as an intermediate (Fig. 8, III and IV). Next, the liberated phosphate is exchanged for SeP at the P-loop (Fig. 8, IV), which would then be ideally situated to donate Se²⁻ to the β -carbon of the aminoacrylate moiety (Fig. 8, IV and V). We suggest that attack of the aminoacrylyl-tRNA^{[Ser]^{Sec} intermediate by SeP involves concomitant attack by a water molecule on SeP, again giving rise to a phosphate leaving group (Fig. 8, IV and V). A general base is proposed to activate this water molecule via a circular protonic shift involving Lys-284 (Fig. 8, IV). Subsequent reverse transaldimination (Fig. 8, V and VI) liberates the product, Sec-tRNA^{[Ser]^{Sec}, and regenerates the internal aldimine.}}}}

Details of the above model are still in the dark. For example, we presently envision sequential binding and conversion of the substrates coupled to repeated contraction and relaxation of the P-loop since our phosphate-soaking experiments only revealed a single phosphate binding site. However, we cannot rigorously exclude the possibility for a separate binding pocket for SeP at the present time. Furthermore, the identity of the water-activating general base is unknown at the time. This function could involve residues from the P-loop/Arg-313 (for example, note the water bound to Arg-97 and phosphate in Fig. 6D). In archaeal SecS, the proposed water activation could be provided by the histidine residue stacking on the PLP. It is also conceivable that Lys-284 directly activates the water molecule without an intervening general base. Evoking a similar scenario, it has been shown that the PLP-binding lysine in *E. coli* cystathionine γ -synthase can reach to distal regions of the substrate (55). Work is in progress to further corroborate and refine this mechanism. To this end, our high resolution crystal structures of *mmu*SecS^{elast} provide excellent leads for further rational site-directed mutagenesis.

Acknowledgments—We thank Elke Penka for excellent technical support, Ralf Ficner, University of Göttingen, for providing generous access to his X-ray diffraction facilities, Richard Glass, University of Arizona, for the precursor used in generating selenophosphate, and Stefano Marino, University of Nebraska, for help with computational analysis.

REFERENCES

- Kryukov, G. V., Castellano, S., Novoselov, S. V., Lobanov, A. V., Zehtab, O., Guigo, R., and Gladyshev, V. N. (2003) *Science* **300**, 1439–1443
- Böck, A., Forchhammer, K., Heider, J., and Baron, C. (1991) *Trends Biochem. Sci.* **16**, 463–467
- Allmang, C., and Krol, A. (2006) *Biochimie (Paris)* **88**, 1561–1571
- Hatfield, D. L., Carlson, B. A., Xu, X. M., Mix, H., and Gladyshev, V. N. (2006) *Prog. Nucleic Acid Res. Mol. Biol.* **81**, 97–142
- Rother, M., Resch, A., Wilting, R., and Böck, A. (2001) *Biofactors* **14**, 75–83
- Leinfelder, W., Zehelein, E., Mandrand-Berthelot, M. A., and Böck, A. (1988) *Nature* **331**, 723–725
- Lee, B. J., Worland, P. J., Davis, J. N., Stadtman, T. C., and Hatfield, D. L.

- (1989) *J. Biol. Chem.* **264**, 9724–9727
- Commans, S., and Böck, A. (1999) *FEMS Microbiol. Rev.* **23**, 335–351
- Forchhammer, K., Leinfelder, W., and Böck, A. (1989) *Nature* **342**, 453–456
- Fagegaltier, D., Hubert, N., Yamada, K., Mizutani, T., Carbon, P., and Krol, A. (2000) *EMBO J.* **19**, 4796–4805
- Tujebajeva, R. M., Copeland, P. R., Xu, X. M., Carlson, B. A., Harney, J. W., Driscoll, D. M., Hatfield, D. L., and Berry, M. J. (2000) *EMBO Rep.* **1**, 158–163
- Heider, J., Baron, C., and Böck, A. (1992) *EMBO J.* **11**, 3759–3766
- Berry, M. J., Banu, L., Harney, J. W., and Larsen, P. R. (1993) *EMBO J.* **12**, 3315–3322
- Copeland, P. R., Fletcher, J. E., Carlson, B. A., Hatfield, D. L., and Driscoll, D. M. (2000) *EMBO J.* **19**, 306–314
- Small-Howard, A., Morozova, N., Stoytcheva, Z., Forry, E. P., Mansell, J. B., Harney, J. W., Carlson, B. A., Xu, X. M., Hatfield, D. L., and Berry, M. J. (2006) *Mol. Cell. Biol.* **26**, 2337–2346
- Xu, X. M., Mix, H., Carlson, B. A., Grabowski, P. J., Gladyshev, V. N., Berry, M. J., and Hatfield, D. L. (2005) *J. Biol. Chem.* **280**, 41568–41575
- Chavatte, L., Brown, B. A., and Driscoll, D. M. (2005) *Nat. Struct. Mol. Biol.* **12**, 408–416
- Hendrickson, T. L. (2007) *Nat. Struct. Mol. Biol.* **14**, 100–101
- Ohama, T., Yang, D. C., and Hatfield, D. L. (1994) *Arch. Biochem. Biophys.* **315**, 293–301
- Forchhammer, K., and Böck, A. (1991) *J. Biol. Chem.* **266**, 6324–6328
- Carlson, B. A., Xu, X. M., Kryukov, G. V., Rao, M., Berry, M. J., Gladyshev, V. N., and Hatfield, D. L. (2004) *Proc. Natl. Acad. Sci. U. S. A.* **101**, 12848–12853
- Leinfelder, W., Forchhammer, K., Veprek, B., Zehelein, E., and Böck, A. (1990) *Proc. Natl. Acad. Sci. U. S. A.* **87**, 543–547
- Guimaraes, M. J., Peterson, D., Vicari, A., Cocks, B. G., Copeland, N. G., Gilbert, D. J., Jenkins, N. A., Ferrick, D. A., Kastelein, R. A., Bazan, J. F., and Zlotnik, A. (1996) *Proc. Natl. Acad. Sci. U. S. A.* **93**, 15086–15091
- Xu, X. M., Carlson, B. A., Irons, R., Mix, H., Zhong, N., Gladyshev, V. N., and Hatfield, D. L. (2007) *Biochem. J.* **404**, 115–120
- Kaiser, J. T., Gromadski, K., Rother, M., Engelhardt, H., Rodnina, M. V., and Wahl, M. C. (2005) *Biochemistry* **44**, 13315–13327
- Gelpi, C., Sontheimer, E. J., and Rodriguez-Sanchez, J. L. (1992) *Proc. Natl. Acad. Sci. U. S. A.* **89**, 9739–9743
- Wies, I., Brunner, S., Henninger, J., Herkel, J., Kanzler, S., Meyer zum Buschenfelde, K. H., and Lohse, A. W. (2000) *Lancet* **355**, 1510–1515
- Xu, X. M., Carlson, B. A., Mix, H., Zhang, Y., Saira, K., Glass, R. S., Berry, M. J., Gladyshev, V. N., and Hatfield, D. L. (2007) *PLoS Biol.* **5**, 0096–0105
- Kernebeck, T., Lohse, A. W., and Grotzinger, J. (2001) *Hepatology* **34**, 230–233
- Yuan, J., Palioura, S., Salazar, J. C., Su, D., O'Donoghue, P., Hohn, M. J., Cardoso, A. M., Whitman, W. B., and Söll, D. (2006) *Proc. Natl. Acad. Sci. U. S. A.* **103**, 18923–18927
- Studier, F. W. (2005) *Protein Expression Purif.* **41**, 207–234
- Hartmuth, K., Urlaub, H., Vornlocher, H. P., Will, C. L., Gentzel, M., Wilm, M., and Lührmann, R. (2002) *Proc. Natl. Acad. Sci. U. S. A.* **99**, 16719–16724
- Otwinowski, Z., and Minor, W. (1997) *Methods Enzymol.* **276**, 307–326
- Schneider, T. R., and Sheldrick, G. M. (2002) *Acta Crystallogr. D Biol. Crystallogr.* **58**, 1772–1779
- Perrakis, A., Morris, R., and Lamzin, V. S. (1999) *Nat. Struct. Biol.* **6**, 458–463
- Murshudov, G. N., Vagin, A. A., and Dodson, E. J. (1997) *Acta Crystallogr. D Biol. Crystallogr.* **53**, 240–255
- Winn, M. D., Isupov, M. N., and Murshudov, G. N. (2001) *Acta Crystallogr. D Biol. Crystallogr.* **57**, 122–133
- Vagin, A., and Teplyakov, A. (2000) *Acta Crystallogr. D Biol. Crystallogr.* **56**, 1622–1624
- Holm, L., and Sander, C. (1995) *Trends Biochem. Sci.* **20**, 478–480
- Schneider, G., Kack, H., and Lindqvist, Y. (2000) *Structure* **8**, 1–6
- Fukunaga, R., and Yokoyama, S. (2007) *J. Mol. Biol.* **370**, 128–141
- Fujii, T., Maeda, M., Mihara, H., Kurihara, T., Esaki, N., and Hata, Y. (2000) *Biochemistry* **39**, 1263–1273

43. Kaiser, J. T., Clausen, T., Bourenkow, G. P., Bartunik, H. D., Steinbacher, S., and Huber, R. (2000) *J. Mol. Biol.* **297**, 451–464
44. Lima, C. D. (2002) *J. Mol. Biol.* **315**, 1199–1208
45. Mihara, H., Fujii, T., Kato, S., Kurihara, T., Hata, Y., and Esaki, N. (2002) *J. Biochem. (Tokyo)* **131**, 679–685
46. Cupp-Vickery, J. R., Urbina, H., and Vickery, L. E. (2003) *J. Mol. Biol.* **330**, 1049–1059
47. Clausen, T., Kaiser, J. T., Steegborn, C., Huber, R., and Kessler, D. (2000) *Proc. Natl. Acad. Sci. U. S. A.* **97**, 3856–3861
48. Sauerwald, A., Zhu, W., Major, T. A., Roy, H., Palioura, S., Jahn, D., Whitman, W. B., Yates, J. R., III, Ibba, M., and Söll, D. (2005) *Science* **307**, 1969–1972
49. Hester, G., Stark, W., Moser, M., Kallen, J., Markovic-Housley, Z., and Jansonius, J. N. (1999) *J. Mol. Biol.* **286**, 829–850
50. Steegborn, C., Clausen, T., Sondermann, P., Jacob, U., Worbs, M., Marinkovic, S., Huber, R., and Wahl, M. C. (1999) *J. Biol. Chem.* **274**, 12675–12684
51. Clausen, T., Huber, R., Laber, B., Pohlenz, H. D., and Messerschmidt, A. (1996) *J. Mol. Biol.* **262**, 202–224
52. Dwivedi, C. M., Ragin, R. C., and Uren, J. R. (1982) *Biochemistry* **21**, 3064–3069
53. Hubert, N., Sturchler, C., Westhof, E., Carbon, P., and Krol, A. (1998) *RNA* **4**, 1029–1033
54. Baron, C., and Böck, A. (1991) *J. Biol. Chem.* **266**, 20375–20379
55. Clausen, T., Huber, R., Prade, L., Wahl, M. C., and Messerschmidt, A. (1998) *EMBO J.* **17**, 6827–6838
56. Lacourciere, G. M., and Stadtman, T. C. (1998) *J. Biol. Chem.* **273**, 30921–30926
57. Notredame, C., Higgins, D. G., and Heringa, J. (2000) *J. Mol. Biol.* **302**, 205–217
58. Davis, I. W., Murray, L. W., Richardson, J. S., and Richardson, D. C. (2004) *Nucleic Acids Res.* **32**, 615–619
59. Krissinel, E., and Henrick, K. (2004) *Acta Crystallogr. D Biol. Crystallogr.* **60**, 2256–2268

SUPPLEMENT

Figure S1: Electron density. Experimental SIRAS electron density (blue mesh) at 2.0 Å resolution after solvent flattening contoured at the 1σ level. *A.* Density covering one molecule of a tetramer. The other three protomers are indicated as light gray ribbons. *B.* SIRAS density of a α -helical element with the final model indicated as yellow ball-and-sticks.

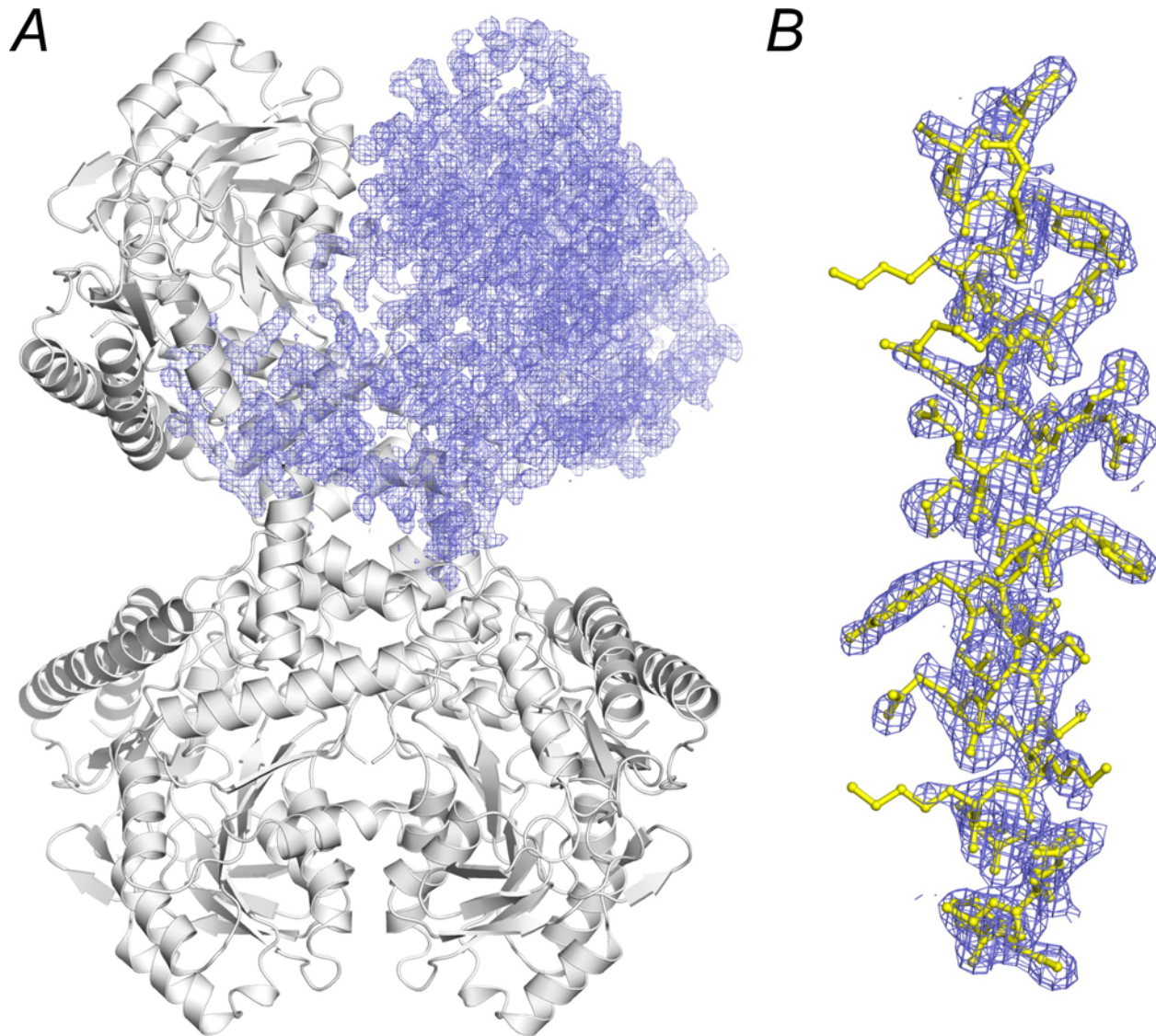


Figure S1